University of Alberta

Separation and analysis of liquid crystalline material from heavy petroleum fractions

by

Brady Kenneth Masik

A thesis submitted to the Faculty of Graduate Studies and Research
in partial fulfillment of the requirements for the degree of

Master of Science
in
Chemical Engineering

Chemical and Materials Engineering

Fall 2011
Edmonton, Alberta

Abstract

Liquid crystalline domains were observed in fractions of heavy petroleum. Through a combination of polarized light microscopy and Photoacoustic Infrared Spectroscopy, liquid crystals were shown to form on the exterior surface of their parent materials. Analysis of materials using Differential Scanning Calorimetry and observations using cross polarized light microscopy both showed that the transition from liquid crystal to isotropic liquid upon heating is irreversible. An enriched sample of liquid crystalline material was extracted from Athabasca bitumen C5 asphaltenes by solvent extraction and analyzed using Fourier Transform Ion Cyclotron Resonance Mass Spectrometry. The enriched sample was shown to have a lower and narrower molecular mass range and higher relative abundances of sulfur, oxygen and nitrogen than the parent asphaltenes. Observations, analysis methods and implications for petroleum separation are discussed in detail.

Acknowledgements

I have to start off with thanking my parents. They have always supported me and encouraged me to be the best person that I can be.

A big thank-you goes to Dr. John Shaw, my supervisor in this work. Without his knowledge, insight and assistance, this thesis would have neither started nor finished.

Thanks to Dr. Murray Gray and Dr. William McCaffrey from the University of Alberta for the use of their laboratories and equipment.

The completion of this work was highly dependent upon external collaborators. My gratitude to them cannot be understated. Thank you to Dr. Kirk Michaelian and Dr. Qing Wen at CANMET Energy in Devon for performing the Photoacoustic Infrared experiments. Dr. Amy McKenna at the National High Magnetic Field Lab at Florida State University performed the mass spectrometry analysis for which I am truly grateful.

It is always a great thing to be surrounded by great people. I was lucky enough to be surrounded by the members of the Petroleum Thermodynamics Research Group. Reza Bagheri deserves special thanks for all of his input to my work, especially starting out. Mildred Becerra also played an important part in helping me perform experiments in the lab.

Finally I have to thank all my friends, too numerous to mention by name. Thank you all for discussing my results with me, help to edit my thesis, and for always being there for me.

Table of Contents

List of Tables

List of Figures

1. Introduction

Petroleum is a complex mixture consisting of tens of thousands of components of diverse types with a broad range of molar masses[1-9]. In crude oil processing, the heavier fractions, and notably asphaltenes are of particular interest. Asphaltenes are traditionally defined as the alkane-insoluble portion of crude oil. They are a material that is not well-understood and topics such as their molar mass and molecular structure are hotly debated among researchers [1-9]. It is not surprising that there is so much being invested in asphaltene research. Asphaltenes play a major role in crude oil processability by depositing as solids that obstruct flow, by increasing viscosity and density, and by stabilizing oil-water emulsions [10]. Asphaltenes also pose problems during heavy oil refining. They can deposit in refinery equipment, limit conversion efficiency, serve as precursors to coke and lead to catalyst deactivation [11]. A more detailed understanding of their properties could lead to significant improvements in production, transport and refining process efficiency.

The recent observation of liquid crystals in petroleum [12] is an important step forward in understanding petroleum phase behaviour. Liquid crystals are an intermediate state between solid and liquid where the liquid can flow but remains ordered or anisotropic in one or two dimensions [13]. The observation that a mixture as complex as petroleum is exhibiting such behaviour could prove to be pivotal in the understanding of its constituents and the development of new research directions linked to novel products, separation techniques and chemical reaction schemes.

Liquid crystal isolation from petroleum, detailed physical structure, and chemical analysis of the liquid crystal forming materials in crude oils are key research targets. Each of these research topics presents significant experimental challenges requiring leading edge techniques and expertise and collaboration and coordination of experiments.

The work that follows is exploratory in nature. The goal is to discover more about the liquid crystals in petroleum - their physical structure, chemical makeup, methods for their isolation. This work will serve as a stepping stone for those who choose to pursue the study of liquid crystals in petroleum and the development of models or equations describing the behaviour of liquid crystals in petroleum.

The thesis comprises six chapters. Chapter 2, which follows the introduction, comprises brief literature reviews on liquid crystals in general as well as in petroleum, isolation of liquid crystals, asphaltene composition, and asphaltene fractionation techniques. Chapter 3 describes the experimental techniques used in this work. The results obtained from each experimental technique are presented in chapter 4 and discussed in

Chapter 5. Conclusions and recommendations for future work are presented in Chapter 6.

2. Literature Review

Overview

This chapter presents brief literature reviews pertinent to the topics addressed during the course of the thesis. Principal topics include: liquid crystals in general and in petroleum in particular as well as separation techniques for liquid crystals. As liquid crystals appear in asphaltenes, asphaltene composition is also reviewed.

Liquid Crystals in General

What are liquid crystals?

When referring to states of matter, the terms solid, liquid and gas are generally what come to mind. However, liquid crystals can form as an intermediate state between a crystalline solid and liquid. A crystalline solid is ordered in three dimensions. A liquid has no long range order and flows. A liquid crystal retains order in one or two dimensions and also has the ability to flow. [13] The transition from solid to liquid crystal states is complex as are the resulting physical states and their properties[14]. Only three basic physical structures are described here.

Columnar liquid crystals have long-range order in two dimensions, like an array of liquid tubes. Smectic liquid crystals have quasilong-range order in one dimension, that is, they are liquid layers stacked on one another. Nematic liquid crystals have positional short range order and orientational long range order[13]. Figure 2-1 shows cartoon depictions of the alignment in each of these phases. It is desirable to determine what type of molecular order the liquid crystals in petroleum exhibit.

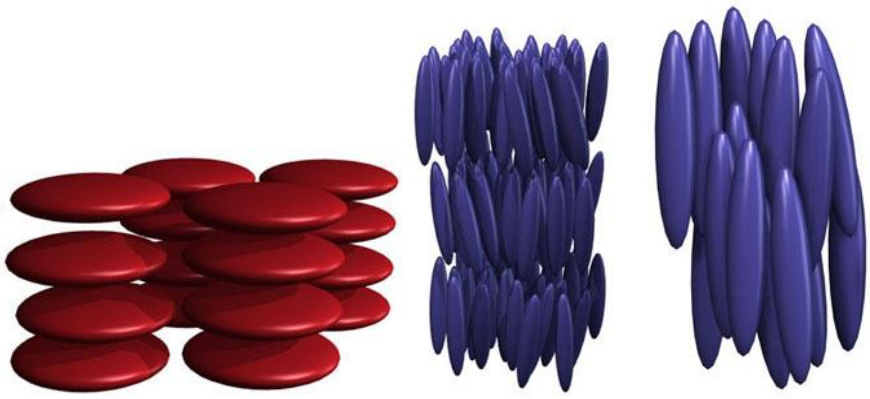

Figure 2-1. Left: Columnar liquid crystals. Middle: Smectic liquid crystals. Right: Nematic liquid crystals. [15]

There are two ways to induce a liquid crystal transition. One way is by varying the temperature. Liquid crystals that form in this way are called thermotropic. Another way to induce a liquid crystal transition is by changing the concentration in a solvent. Liquid crystals that form in this fashion are called lyotropic.[13] Compounds that exhibit liquid crystalline transitions with both temperature and composition variation are called amphotropic.

Types of molecules that form liquid crystals

There are several classes of molecules that are known to form liquid crystals: small elongated organic molecules, small discoid organic molecules, and long helical rods [13]. There are many examples of liquid crystals that exist in the molar mass range of asphaltenes and other petroleum fractions. Table 2-1 lists examples of compounds known to form liquid crystals. Some of the molecules have multiple possibilities for side chains. These possibilities are presented in Tables 2-2 and 2-3.

Table 2-1. Liquid crystal forming compounds

Compound	**Molar Mass (g/mol)**	**Source**
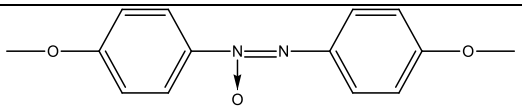 *p*-azoxyanisole	258.10	[13]
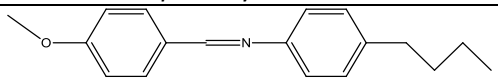 *N*-(*p*-methoxybenzylidene)-*p*-butylaniline	267.16	[13]
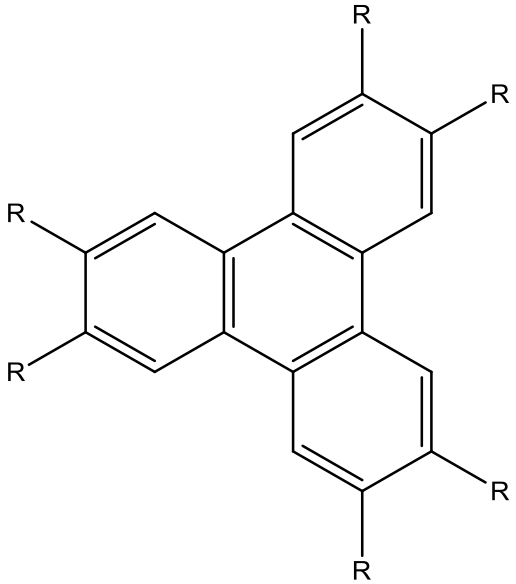 General discotic molecule For details on R see Table 2-2.	>300	[13]

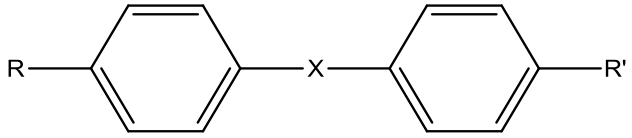 Elongated molecule. For details on R, X and R' see Tale 2-3.	>200	[13]
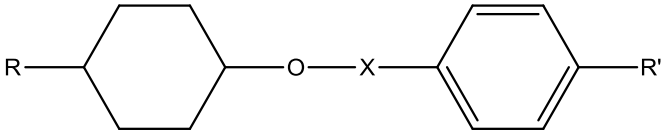 Elongated molecule. For details on R, X and R' see Table 2-3.	>200	[13]
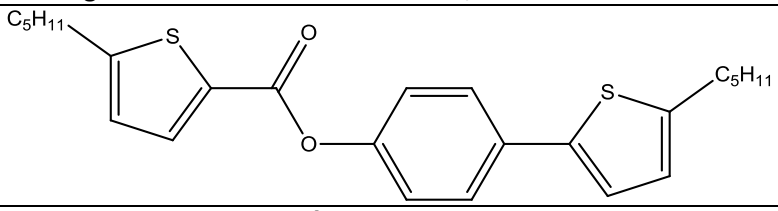	426.17	[16]
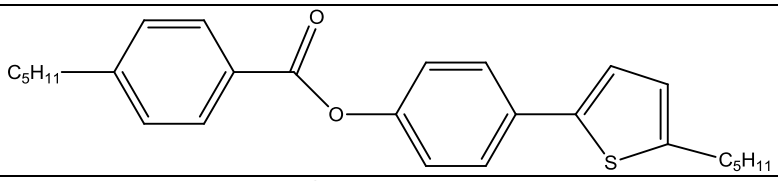	420.21	[16]
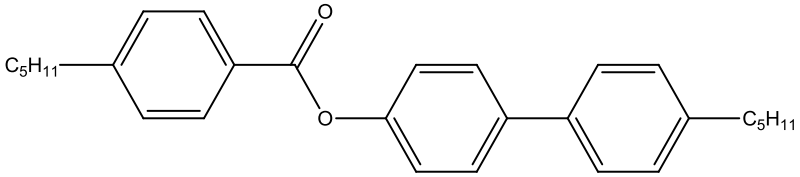	414.26	[16]
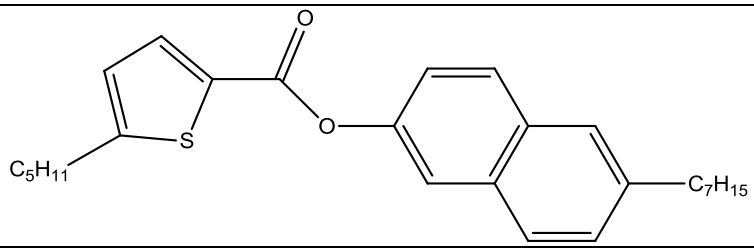	422.23	[16]
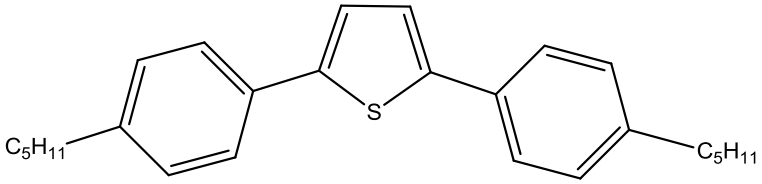	376.22	[16]
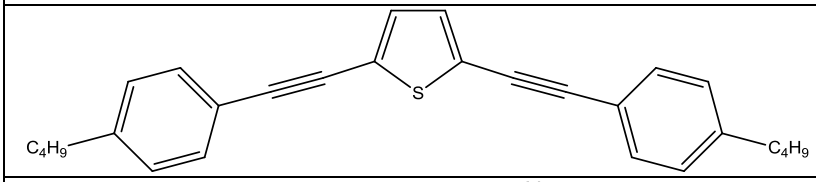	396.19	[16]
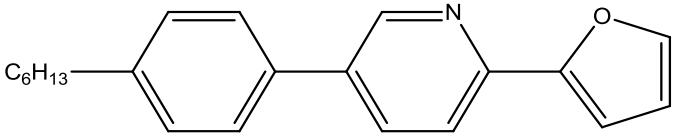	305.18	[17]

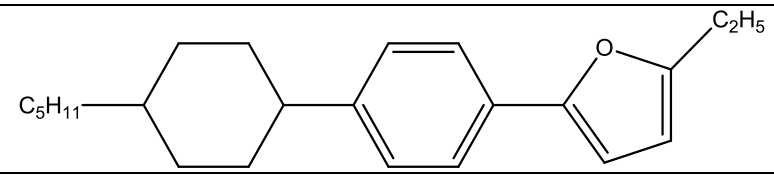	324.25	[17]
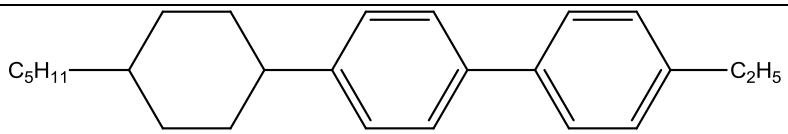	334.27	[17]
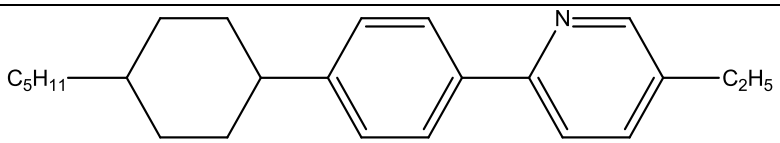	335.26	[17]
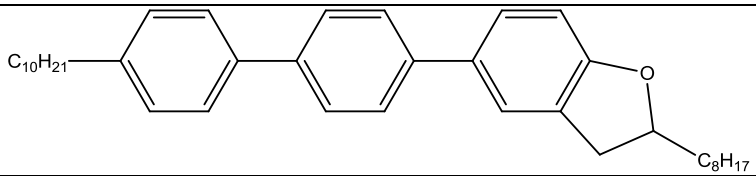	524.40	[17]
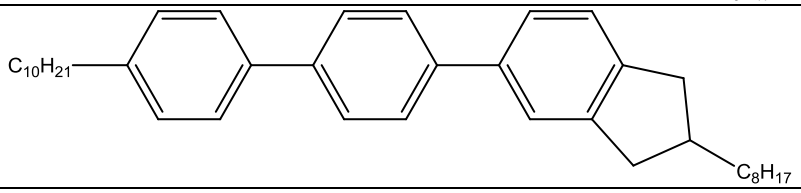	522.42	[17]
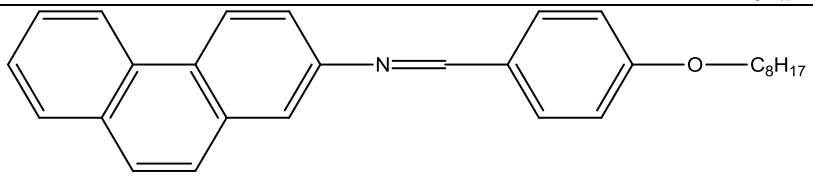	409.24	[17]
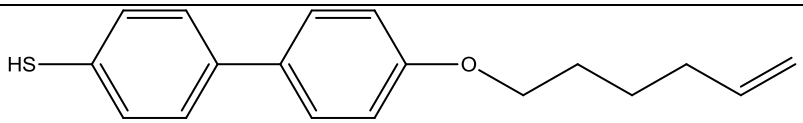	284.42	[18]

Table 2-2. Example structures for R for discotic molecules listed in Table 2-1 [13].

Designation	**R**
a	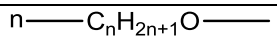
b	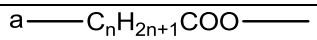
c	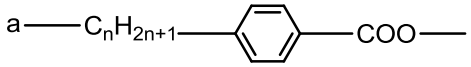
d	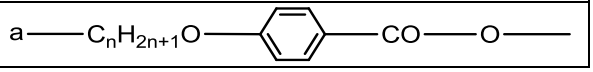

Table 2-3. Examples of R, X and R' for small elongated molecules[13]. For more examples see [13].

R	X	R'
C_nH_{2n+1} –	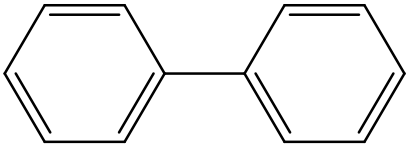	R
$C_nH_{2n+1}O$ –	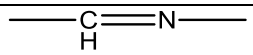	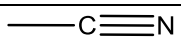
$C_nH_{2n+1}COO$ –	– COO –	– Cl
$C_nH_{2n+1}OCOO$ –	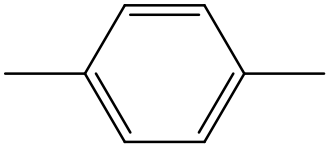	– Br
	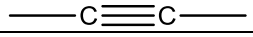	– F
		– NO_2

References [16] and [17] have many more examples of liquid crystal forming compounds, however, those listed in Table 2-1 are chosen because they fit well within the molar mass range for asphaltenes and heavy petroleum fractions.

Liquid crystal isolation

There are many methods that are commonly used for the isolation of chemicals. These methods include but are not limited to: solvent extraction, recrystallization, sublimation, and chromatography. In some cases the techniques are combined in multiple steps to obtain desired purities. [19]

Solvent extraction involves selecting a suitable solvent to dissolve a material of interest from a mixture. The solvent is then evaporated and the material is collected [19]. Extraction is often performed with two immiscible liquid phases (liquid-liquid extraction), but can also be used to selectively extract materials from a solid mixture. The important part of solvent extraction is to select a solvent in which the material of interest is soluble, and the rest of the mixture is insoluble. [19]

During sublimation, the pressure over a solid is reduced to induce part of solid to sublime. After the vapour travels a short distance away from the original solid, it is condensed onto a cooled surface. The technique is used to purify many inorganic solids such as aluminum chloride, ammonium chloride, arsenious oxide and iodine. [19]

Chromatography is a technique that is used for the purification of small amounts of complex organic mixtures [19]. It relies on the differential distribution of the components in a mixture between a mobile phase and a stationary phase where the

mobile phase is either a gas or a liquid, and the stationary phase is a solid or a non-volatile liquid adsorbed on a solid surface [19]. In High performance liquid chromatography (HPLC) the mobile phase is a liquid and the stationary phase coats or comprises packing in a column. HPLC employs a hydraulic system to provide pressure, a column with packing, a detector, data storage and output. The packing may be an absorbent, a material impregnated with a high boiling liquid, an ion-exchange material, or a highly porous non-ionic gel [19]. The mobile phase can be water, aqueous buffers, salt solutions, organic solvents or mixtures of these [19]. There are a wide range of HPLC columns available for different applications.

Solvent recrystallization is a standard technique for the purification of crystalline materials. Recrystallization depends on finding a solvent in which the desired compound has a high solubility at high temperature and a low solubility at low temperature. The solvent must be saturated at the high temperature, and when it is cooled the desired compound will crystallize first. The crystals that form should be a relatively pure form of the desired compound. As liquid crystals are crystalline in the solid state, solvent recrystallization is commonly used as a method for their purification. More detail on the solvent recrystallization technique can be found elsewhere [19].

For example, the liquid crystal forming compound *N*-(*p*-methoxybenzylidene)-*p*-butylaniline (MBBA) is produced in relatively high purity simply by chemical reaction that proceeds nearly to completion [20]. If higher purity is desired it can be achieved through solvent recrystallization [21]. For compounds that are not produced in high purity the recrystallization step is necessary to obtain a sizeable sample. An example of such a compound is cholesteryl benzoate which must be recrystallized from ethyl acetate [21]. If solvent recrystallization does not give a pure enough product, it has been shown that zone refining (a process which uses melting and refreezing to eliminate impurities) can potentially be used to further purify liquid crystals [22].

With the use of a suitable solvent either recrystallization or extraction could prove to be useful techniques in the separation of the liquid crystal forming material from petroleum. These techniques are favourable compared to the others due to their simplicity and ease of application on a laboratory scale.

Liquid crystals in Petroleum

The formation of mesophase and liquid crystals in refined petroleum, materials subject to chemical reaction, is well documented. A common example of liquid crystals forming in petroleum is found in carbonaceous mesophase[23-28]. Carbonaceous mesophase forms when pitch is heated in the temperature range of 350-500°C and is an intermediate product in the coking process [25]. It is considered to be a nematic discotic liquid crystal. That is, the molecules are disc-like and form a worm-like texture. Carbonaceous mesophase forms due to molecular weight growth processes that create

large planar polyaromatic compounds with molar masses in the 500 – 2000 Da range [25]. The liquid crystals in carbonaceous mesophase are different from those observed in [12] and [29] since it is formed due to a chemical reaction. Liquid crystal rich material has been separated from pitch using supercritical toluene [30] and pentane [31].

Amphotropic liquid crystals, the subject of this work, have only been observed recently in unreacted petroleum fractions [12]. These latter liquid crystals have been shown to form from a variety of sources including Athabasca asphaltenes, Maya asphaltenes, Cold Lake asphaltenes, Safaniya asphaltenes and a fraction of Athabasca bitumen extracted with supercritical n-pentane. The liquid crystals form between 338 and 341 K for C5 asphaltenes depending on the source, 371 K for C7 Safaniya asphaltenes, and 316 K for a fraction of Athabasca bitumen extracted with supercritical n-pentane. The liquid crystals disappear at 423 to 435 K for C5 asphaltenes depending on the source, 433 K for C7 Safaniya asphaltenes, and 373 K for the fraction of Athabasca bitumen extracted with supercritical n-pentane. These materials also exhibit liquid crystalline domains in the presence of toluene vapour at room temperature. [12]

A liquid crystal phase has also been observed at oil-water interfaces[29, 32] and it has been theorized that this phase plays a role in the stabilization of water-in-oil emulsions [29]. A sample of this interfacial material was collected by centrifuging heavy water (D_2O) droplets in oil suspended over a regular water layer. The heavy water droplets with the interfacial material form a cake at the bottom of the centrifuge cell. The cake was collected and its composition analyzed by Fourier Transform Ion Cyclotron Resonance Mass Spectrometry (FT-ICR MS). The result showed a composition different from asphaltenes, resins, and the parent oil with molecules containing significant mass fractions of oxygen and sulfur. [32]

Asphaltene Composition

As the liquid crystals separated from the heavy petroleum and investigated in detail were derived from C5 asphaltenes, it is important to review what is known about them. Their elemental composition is easily determined [33], but the molecular composition [2, 3, 34-39] and average molecular weight [2-8] remain points of contention among researchers. A wide range of molar masses is to be expected since asphaltenes consist of many different compounds of diverse types. Nearly 30,000 peaks are detected for Athabasca C7 asphaltenes using FT-ICR MS [40]. The molecular structures of the compounds are poorly defined. With a portion of asphaltenes exhibiting liquid crystalline behaviour, a fraction of asphaltenes must contain molecules that share structural elements with compounds that are known to exhibit liquid crystalline behaviour.

Asphaltene Fractionation

A method that has been used for the fractionation of asphaltenes is Soxhlet extraction using heptol in various concentrations as a solvent [41]. This method could be useful in extracting the liquid crystals from asphaltenes but requires a large quantity of asphaltenes making it impractical for small scale application. Multi-stage approaches have been used in which pentane is added step-wise as an antisolvent to precipitate asphaltenes from a solution in toluene [42] or methylene chloride [43]. This anti-solvent approach may produce a fraction that is rich in liquid crystal forming material.

Objectives

The goal of this exploratory work is to provide insights into the structure, mass fraction and behaviour of liquid crystals previously observed in heavy petroleum. There are several lines of inquiry: What is the physical structure of the liquid crystals? Where are the liquid crystals when they form? What factors affect the formation of liquid crystals? Which petroleum fractions have the highest proportion of liquid crystal forming materials? How can an enriched sample of liquid crystals be produced? What is the chemical make-up of the liquid crystals?

Each line of inquiry presents numerous challenges. Some are addressed in a qualitative and others in a more quantitative manner in subsequent chapters.

3. Experimental

Overview

Multiple steps were required for the investigation of liquid crystals as performed in this study – detection, isolation/preparation, and analysis. The simplest means of detection was via polarized light microscopy. This method allows for easy observation of liquid crystalline behaviour. Once the liquid crystals were detected, other forms of analysis were performed that required analytical technique dependent sample preparation. For example, for photoacoustic infrared spectroscopy depth profiling studies, liquid crystals had to be frozen after they formed to preserve spatial orientations. This allowed for determination of the location of the liquid crystal phase relative to the isotropic phase. For analysis of bulk sample properties e.g.: using Differential Scanning Calorimetry or Fourier Transform Ion Cyclotron Resonance Mass Spectrometry, preparation of samples enriched in liquid crystal forming material were preferred.

Materials

Laboratory Chemicals

Several laboratory chemicals were used in this work: heptane (Assay 99.5%, Fisher Scientific), pentane (Assay 99.6%, Fisher Scientific) and toluene (Assay 99.9%, Fisher Scientific).

Model Liquid Crystal

A sample of 4-Isothiocyanatophenyl 4-pentylbicyclo[2,2,2]octane-1-carboxylate ($C_{21}H_{27}NO_2S$) was purchased from Sigma Aldrich to serve as a control for pure liquid crystalline behaviour. It is a nematic liquid crystal in the temperature range between 74.5°C and 113.5°C [44]. At higher temperatures it is an isotropic liquid and at lower temperatures it is a crystalline solid. It was chosen because it has similar phase transition temperatures to the liquid crystals observed in petroleum.

Oil Sample

Athabasca bitumen from Alberta, Canada was obtained from Syncrude Canada Ltd. The sample was characterized as a coker feed. It was derived from mined bitumen subjected to warm water extraction, naphtha dilution, and naphtha recovery by distillation between (523 and 623) K. Some volatile components initially present in the as mined bitumen were lost during processing.

Sample Preparation

Table 3-1 summarizes the samples prepared as part of this work. Each sample is described in detail below.

Source Material

Asphaltenes and maltenes were prepared by precipitation with pentane according to the following procedure. Athabasca bitumen pentane (C5) asphaltenes were precipitated at room temperature and atmospheric pressure by the addition of pentane to bitumen at a ratio of 40:1 by volume. The mixture was covered and stirred overnight at room temperature and then filtered in two steps by vacuum filtration. The first filtration step used a Fisher brand filter paper Q2 with a pore size between 1 and 5 µm. The second filtration step used a 0.22 µm Millipore membrane comprising mixed cellulose esters. The filtration membranes and the flask were washed with small volumes of pentane to eliminated residual oil until the filtrate became colourless. The membranes with precipitated material (pentane asphaltenes) were dried at 373 K for 30 minutes and then placed overnight in a vacuum oven at 9 kPa. Permeate samples were distilled at 313 K to remove pentane and produce pentane maltenes. Heptane (C7) asphaltenes were also prepared using the above procedure where pentane was replaced with heptane. In this work, the Athabasca bitumen C5 asphaltenes are simply referred to as C5 asphaltenes. Similarly the Athabasca bitumen C7 asphaltenes are referred to as C7 asphaltenes.

A sample of an Athabasca bitumen vacuum residue fraction extracted using supercritical pentane [31] and described elsewhere [12] as having large liquid crystal regions forming at a lower temperatures than in other observed petroleum fractions was also available for this study. The vacuum residue was fractionated under the following conditions: the extraction section was maintained at a temperature of 473 K; the fractionation section was maintained at a temperature of 483 K; the pressure of the supercritical fluid began at 3.5 MPa and was increased linearly to 12 MPa over 8 hours. The procedure resulted in the production of 10 fractions, named #1 through #10. Fraction #6, referred to here as SFE6, was extracted from pressures between 8 and 9 MPa.

In order to observe the behaviour of the liquid crystals using transmitted or reflected light, in the presence of other materials, samples were prepared on flat aluminum and glass surfaces. A thin layer of powdered sample was spread evenly across the surface with a spatula. For the liquid crystals to form, the sample was heated in an oven for one hour in air. Different samples required different temperatures. For C5 asphaltenes, the temperature was 145°C. For SFE6, the temperature was 60°C. After this treatment the liquid crystals could be observed using cross polarized light microscopy or photoacoustic infrared spectroscopy.

To observe liquid crystals in C5 maltenes using a light microscope, cooling with liquid nitrogen was required as maltenes are liquid at room temperature. Droplets of

maltenes were placed on an aluminum surface, then immediately immersed in liquid nitrogen. Next the material was crushed and its optical behaviour was observed as it returned to room temperature. Some ice condensed on the sample at the low temperature, so when it was observed under the microscope regions where the moisture condensed were avoided.

Liquid Crystal Enrichment

To analyze liquid crystal behavior and composition in detail, raw samples were enriched using a variety of techniques. Some were more successful than others as noted here.

Heptane soluble portion of pentane asphaltenes

As pentane asphaltenes comprise ~ 19 wt % and heptane asphaltenes comprise ~ 14 wt % of Athabasca bitumen, one avenue explored was to evaluate whether liquid crystals were more concentrated in the heptane soluble fraction of pentane asphaltenes. In this method, C5 asphaltenes were dissolved in heptane at a ratio of 40 mL of heptane for each gram of solid. The mixture was agitated for 24 hours at room temperature and the solids were filtered out. The filtrate was retained and the solvent was evaporated at 95°C. The solid was then crushed and any remaining solvent was evaporated under vacuum at 60°C. The solid that remained afterwards was examined. This approach did not produce a sample that showed any difference in liquid crystalline behaviour over C5 asphaltenes and it was abandoned.

Physical separation

This approach involved the manual manipulation of liquid crystals within the bulk material. The tools used were a heated glass microscope slide and a fine tipped glass rod. The tip of the glass rod was approximately 50 µm in diameter. SFE6 was used as a starting material for this method, since it exhibits the largest regions of liquid crystals. The SFE6 sample was placed on a heated slide and the temperature was set to 60°C. Once the liquid crystals formed, the glass rod was touched to the liquid crystals. Liquid crystal rich material froze to the rod, and the rod was then rinsed in a vial of toluene. From prior work[12], the liquid crystals are known to dissolve in toluene. While this technique worked, the liquid crystals were too small to collect more than microgram quantities of enriched material with multiple repetitions and the samples were found to be too contaminated for FTICR analysis [45], a key use for enriched samples.

Dissolution in solvent following heat treatment

C5 asphaltenes were spread onto a glass microscope slide (Figure 3-1) and then heated to 145°C in air for one hour so the liquid crystals would form. The slide was then cooled and the liquid crystals froze in place. The slide was then treated with a solvent at room temperature. The first two solvents used were heptane and toluene. When the slide was immersed in heptanes for 30 minutes, there was no effect. The liquid crystals remained on the slide. Upon immersion in toluene, materials on the slide immediately dissolved/dispersed.

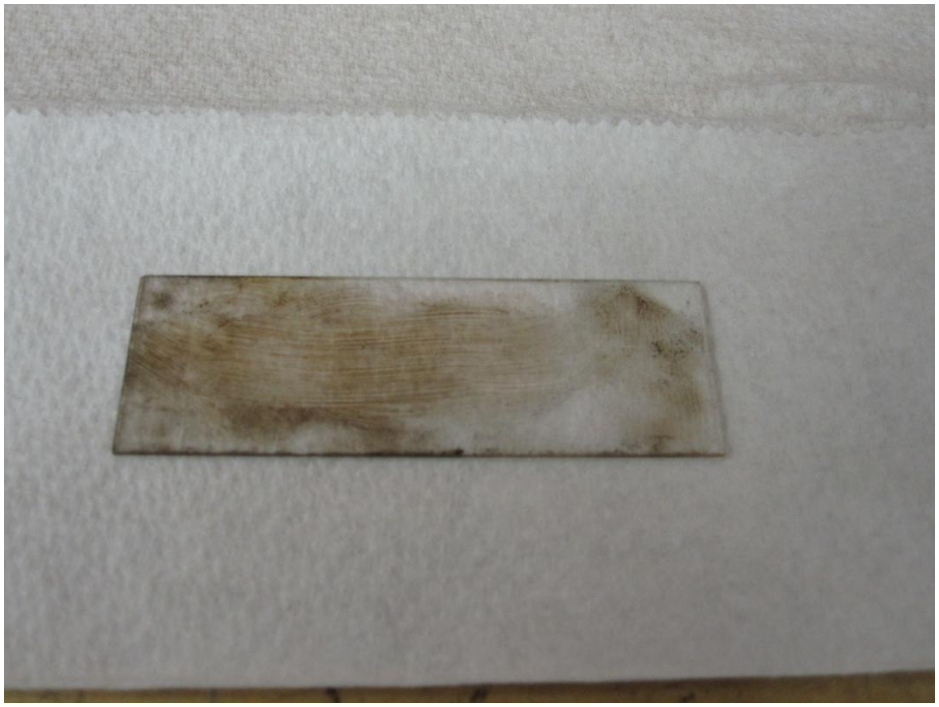

Figure 3-1. Asphaltenes spread on glass microscope slide to prepare for heat and solvent treatment.

The next solvent investigated was a mixture of heptane and toluene. Based on the previously observed behaviour of rapid dissolution/dispersion in toluene, the mixture chosen was 90% heptane and 10% toluene by volume. After the slide was immersed in this solvent for 30 minutes, the solvent displayed a slight change in colour. Different immersion times did not appear to have an effect on the extraction. Observation of the slide under the microscope after treatment showed that much material remained on the slide, but the liquid crystals were gone. Figure 3-2 shows a microscope image of the slide after this treatment. Reheating the material on the slide showed smaller and fewer liquid crystals than were originally in the C5 asphaltenes. The liquid crystals dissolved into the heptane/toluene mixture. The solvent was subsequently evaporated at 95°C and the solid film remaining on the walls of the beaker was retained for further investigation and analysis.

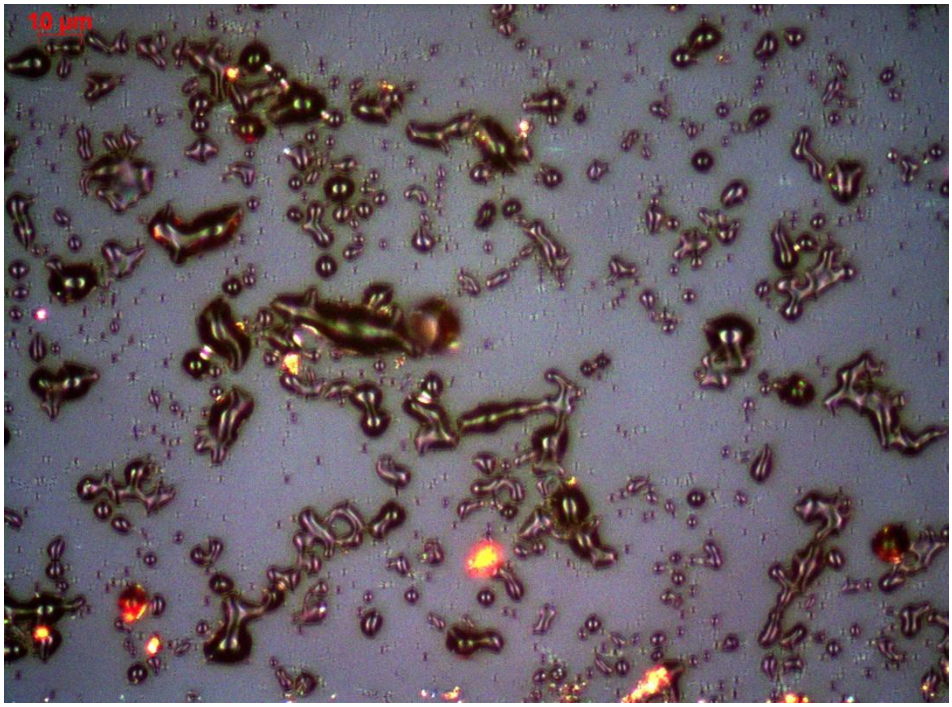

Figure 3-2. Microscope image of slide immediately after solvent treatment at room temperature. No liquid crystals remain visible.

This successful enrichment method was scaled up using a Wheaton Glass Staining Dish that held 8 microscope slides at a time while being immersed in a solvent as shown in Figure 3-3. After a 1 hour heat treatment at 145°C, the slides were placed in the rack and submerged in solvent for 30 minutes. Each batch began with approximately 100 mg of asphaltenes and yielded approximately 5 mg of enriched liquid crystalline sample. This gives a mass fraction of liquid crystal forming material of approximately 5%. The entire sample was not usable as it was obtained as a film on a beaker. Complete removal was not possible.

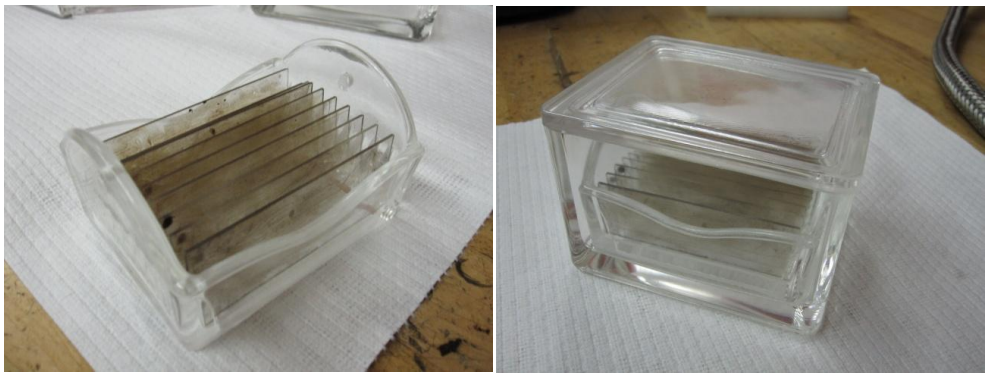

Figure 3-3. Left: Rack to hold multiple slides. Right: Bath to immerse rack in solvent.

Table 3-1. Summary of samples used in this work.

Sample	Description	Origin
C5 asphaltenes	Asphaltenes precipitated using pentane	Athabasca bitumen
C7 asphaltenes	Asphaltenes precipitated using heptane	Athabasca bitumen
C5 maltenes	Oil that did not precipitate from pentane	Athabasca bitumen
SFE6	Fraction of vacuum residue extracted using supercritical pentane	Athabasca bitumen
Liquid crystal enriched	Liquid crystals extracted from C5 asphaltenes	Athabasca bitumen

Experimental Methods

Polarized Light Microscopy

Polarized light microscopy is a useful technique when studying anisotropic materials such as liquid crystals. The technique causes anisotropic regions to appear bright, while isotropic regions are dark. As a result, ordered materials are easy to identify.

The microscope works by having two polarizing filters, termed the polarizer and the analyzer. Light first passes through the polarizer and illuminates the sample. The analyzer is placed between the observer and the sample and its direction of polarization is perpendicular to the initial polarizer[46]. If the sample is isotropic, then the direction of polarization will be unchanged and appear dark to the observer. If the sample is anisotropic, as in liquid crystals, the direction of polarization will be changed and the material will appear bright. Figure 3-4 shows a schematic of how the polarized light microscope works.

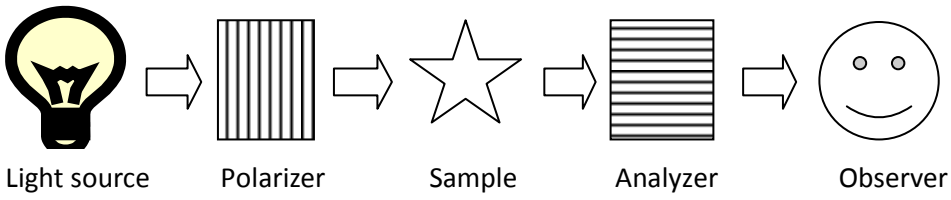

Figure 3-4. Schematic of how a polarized light microscope works.

The technique is useful for quick identification of anisotropic materials. It is also useful for determining how the materials behave through phase transitions. The technique was also used in this work to estimate the relative quantity of liquid crystalline material in each sample compared with other samples.

Figure 3-5 shows an example of what liquid crystals can look like through a cross polarized light microscope. The black regions are isotropic. If the entire sample is isotropic, the entire image would appear dark.

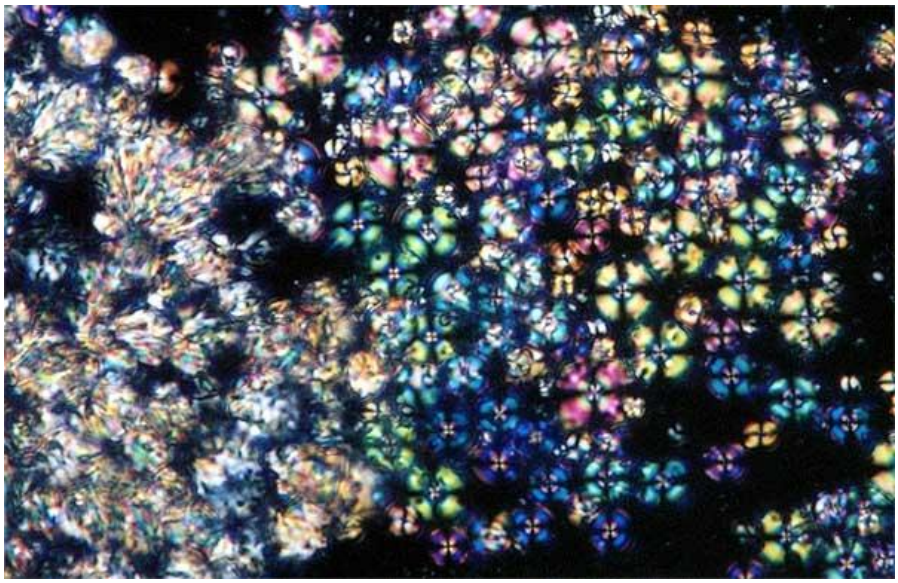

Figure 3-5. Liquid crystals through a cross polarized light microscope. The left side shows a nematic texture, the right side is smectic. Temperature conditions are different on each side of the image causing the transition to be visible. [47]

Differential Scanning Calorimetry

Differential Scanning Calorimetry (DSC) is a method that tracks the heat flow to a sample as a function of temperature. This is done by comparing the amount of heat required to raise the temperature of a sample to an empty reference cell. The technique allows for detection and tracking of phase transitions as well as determination of heat capacities. [48]

To perform the experiment, two cells are required – an empty reference cell and a second cell with variable content. To obtain data for any given sample, three experiments must be performed. In the first experiment, the second cell is empty. In the second experiment, the second cell contains a calibration material. In this case, the calibration material was sapphire. Finally, the experiment is run with the desired sample in the second cell. For accurate results, a mass of sample of approximately 50 mg is desired. This amount of sample gives results with less noise than a miniscule (<10 mg) amount of sample. The temperature of the sample and reference cells is increased

at the same rate and the difference in heat flow is measured. If the sample undergoes a phase transition it will be observed as a peak on the DSC heat capacity curve. The direction of the peak shows whether the transition was exothermic or endothermic. The area under the peak region shows the enthalpy of the transition.

In this work, apparent heat capacities were measured using a differential scanning calorimeter TG-DSC 111 (Setaram, France). A heating-rate dependent temperature calibration to ITS-90 was performed using indium, tin, lead, zinc (mass fractions 0.99999, Sigma-Aldrich Co.), naphthalene (mass fraction 0.997, Sigma-Aldrich Co.), gallium (mass fraction 0.999995, Sigma-Aldrich Co.) and cyclohexane (mass fraction 0.9999, Sigma-Aldrich Co.). Octane (mass fraction 0.998 determined by GC, Fluka/Sigma-Aldrich Co) and decane (mass fraction 0.9999 determined by GS, Fluka/Sigma-Aldrich Co.) were used for calibration of the temperature range down to 200 K due to their well-defined triple points. The energy calibration was performed with the Joule effect method in the factory and checked by measuring the enthalpy of fusion of gallium, naphthalene, indium and tin. Accuracy was found to be within 1% of literature values. Measured enthalpies of fusion for octane and decane agreed within 2% of the literature values. Heat capacity calibration was performed using naphthalene and synthetic sapphire. The uncertainty of the heat capacity measurements was less than 10% in the temperature range of 190 K to 220 K, less than 6% from 220 K to 240 K, about 3% from 240 k to 280 K, and less than 2% from 290 K to 570 K. Random device artifacts made the temperature range from 280 K to 290 K unreliable.

DSC measurements were performed on C5 asphaltenes from 293 K to 473 K, SFE6 from 273 K to 473 K and the model liquid crystal ($C_{21}H_{27}NO_2S$) from 293 K to 473 K. There was not enough of the liquid crystal enriched sample collected for DSC analysis.

Photoacoustic Infrared Spectroscopy

Photoacoustic infrared (PA-IR) spectroscopy is a technique used to obtain an infrared spectrum for a sample. The technique is convenient and useful as little sample preparation is required, it is suitable for opaque materials, depth profiling can be performed, and it is not destructive [49]. The technique can be simplified to four main steps. A modulated infrared laser is aimed at the sample, the sample heats up due to the laser, the heat causes a pressure wave in the gas above the sample which is detected by a microphone, and finally a Fourier transform is applied to the microphone signal to obtain the infrared spectrum. The technique is described in detail in reference [49]. By varying the modulation frequency of the laser beam, different layers of the sample can be analyzed. This is a very useful property of PA-IR spectroscopy that can be applied when analyzing liquid crystals. It allows analysis of the different parts of the liquid crystal droplets.

The PA-IR experiments yield an infrared spectrum. Further analysis is performed on the spectrum. For depth profiling of non-uniform samples, different modulation

frequencies yield different spectra for varying depths. A sample of oil sand prepared at Syncrude Canada Ltd. using Dean-Stark distillation is used to exemplify results from PA-IR analysis [50]. The sample was collected in a thimble at the bottom of the extraction column and is hence named Syncrude thimble solids. Figure 3-6 shows an example of PA-IR spectra obtained from Syncrude thimble solids [50].

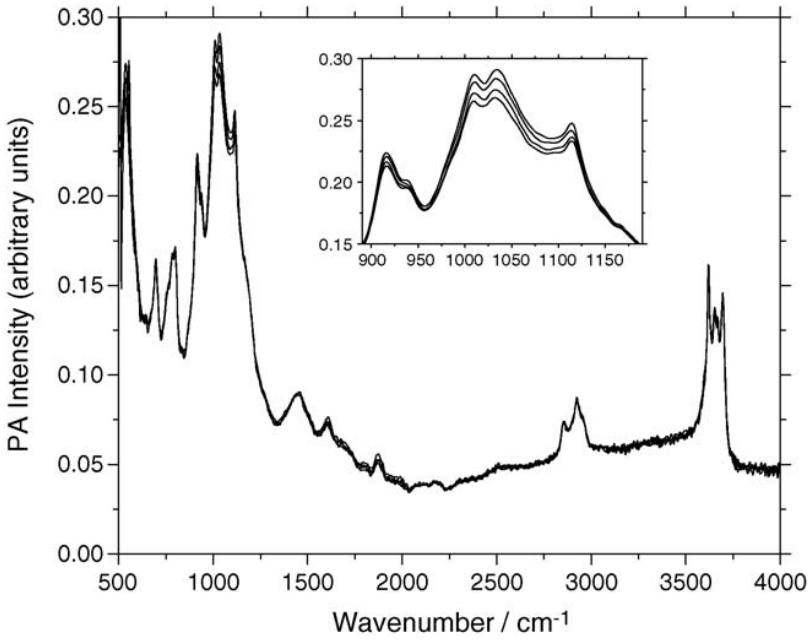

Figure 3-6. PA-IR spectra for Syncrude thimble solids. Four curves are present for modulation frequencies of 3.716, 4.42, 5.26 and 6.25 kHz listed from bottom to top. Reprinted from [50]. Copyright 2006, with permission from Elsevier.

Integrating selected regions of interest allows for comparison of spectra. In [50] the kaolinite (clay) region at 852 to 1300 cm^{-1} and the hydrocarbon region at 2800 to 3000 cm^{-1} were compared. The area of the kaolinite region was divided by the area of the hydrocarbon region to determine the ratio of kaolinite to hydrocarbon. Figure 3-7 shows the kaolinite to hydrocarbon ratios plotted against various modulation frequencies for Syncrude thimble solids[50].

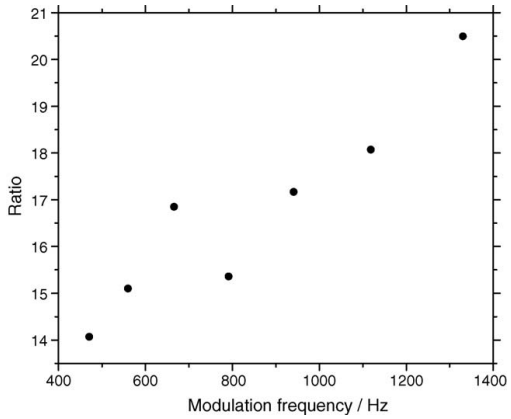

Figure 3-7. Modulation frequency plotted against kaolinite to hydrocarbon ratio for Syncrude thimble solids. The modulation frequency is specified at a wavenumber of 2000 cm^{-1}. Reprinted from [50]. Copyright 2006, with permission from Elsevier.

The modulation frequency can be converted to thermal diffusion length (μ_s) using the relationship $\mu_s = (\alpha/\pi f)^{1/2}$ where α (cm^2/s) is the thermal diffusivity of the sample and f (Hz) is the modulation frequency[50]. Thermal diffusivity can be assumed to be 0.001 cm^2/s for post-extraction oil sand samples[50]. This assumption simplifies the relationship $\mu_s = 180 \times f^{-1/2}$. Applying this relationship to the data in Figure 3-7 allows for visualization of the differences in composition at different depths in the sample. Figure 3-8 shows the kaolinite to hydrocarbon ratio plotted against thermal diffusion length for Syncrude thimble solids [50].

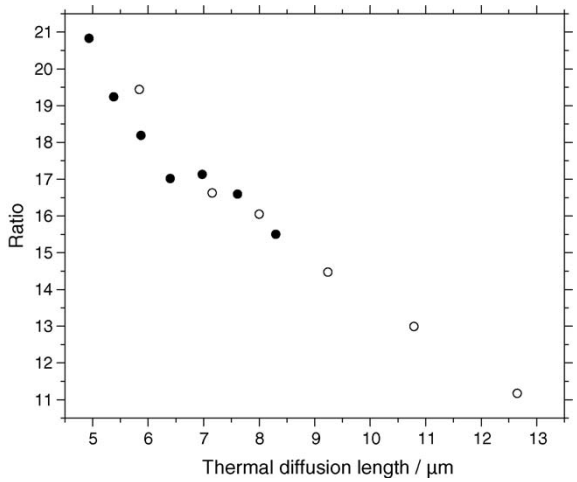

Figure 3-8. Thermal diffusion length plotted against kaolinite to hydrocarbon ratio for Syncrude thimble solids. Solid circles are data obtained using a Bruker IFS 113s FT-IR spectrometer; filled circles are data obtained using a Bruker IFS 66v/S spectrometer at the Canadian Light Source. Reprinted from [50]. Copyright 2006, with permission from Elsevier.

For the depth profiling experiments performed in this work, powdered SFE6 was heat treated on an aluminum surface at 60°C so liquid crystal droplets would form and depth profiling was then performed. Depth profiling was also performed on SFE6 and Athabasca bitumen C7 asphaltenes in KBr that were not heat treated. These latter data were used for comparison purposes.

PA-IR was also performed on bulk samples of both Athabasca bitumen C5 and C7 asphaltenes that had been treated in various ways to obtain an infrared spectrum. Experiments were performed using a Bruker IFS 88 FT-IR spectrometer and an MTEC 200 PA cell at ambient temperature and pressure. For the standard (non-depth profiling) experiments a laser modulation frequency of 1.6 kHz was used. For each experiment, the spectrometer was purged with dry nitrogen gas to reduce interference by ambient water vapour and carbon dioxide during the measurements. Details of the experimental technique can be found elsewhere [51]. Table 3-2 presents the different samples that were analyzed using PA-IR. The region of the spectrum of particular interest was the aromatic C-H region at 3050 cm^{-1}. The area of this region as a fraction of the total area of the C-H stretching region from 2760 cm^{-1} to 3100 cm^{-1} was used as a means for comparison between different samples.

Table 3-2. Samples used for PA-IR

Starting Material from Athabasca bitumen	**Treatment**	**Shorthand Abbreviation**
C5 Asphaltenes	No treatment	C5
C5 Asphaltenes	Crushed	C5 c
C5 Asphaltenes	Heat treated	C5HT
C5 Asphaltenes	Heat treated then crushed	C5HT c
C5 Asphaltenes (solids free)	No treatment	C5NSF
C5 Asphaltenes (solids free)	Crushed	C5NSF c
C5 Asphaltenes (solids free)	Heat treated	C5NSFHT
C5 Asphaltenes (solids free)	Heat treated then crushed	C5NSFHT c
C7 Asphaltenes	No treatment	C7
C7 Asphaltenes	Crushed	C7 c
C7 Asphaltenes	Heat treated	C7HT
C7 Asphaltenes	Heat treated then crushed	C7HT c
C7 Asphaltenes (solids free)	No treatment	C7NSF
C7 Asphaltenes (solids free)	Crushed	C7NSF c
C7 Asphaltenes (solids free)	Heat treated	C7NSFHT
C7 Asphaltenes (solids free)	Heat treated then crushed	C7NSFHT c

All PA-IR measurements were performed by Dr. K. Michaelian's team at the CANMET laboratory in Devon, Alberta.

Fourier Transform Ion Cyclotron Resonance Mass Spectrometry

Fourier Transform Ion Cyclotron Resonance Mass Spectrometry (FT-ICR MS) is a tool to yield a mass spectrum for complex mixtures with a resolution (M/ΔM) of 450000 – 500000 at a mass to charge ratio of 500.

The FT-ICR MS technique can be separated into several distinct steps: ionization, ion accumulation, ion transmission, mass-to-charge (m/z) ratio selective ejection, dipolar excitation, detection, fast Fourier transformation, magnitude computation, and frequency to m/z conversion [52]. The ionization method used was atmospheric pressure photoionization (APPI) because it can ionize low-polarity and nonpolar compounds. Since so many types of compounds are ionized, a complex mass spectrum is produced [53]. The complexity is overcome through the use of a high resolution analyzer – FT-ICR MS. More details about the FT-ICR MS technique can be found in [52-55]. Figure 3-9 shows the configuration of FT-ICR mass spectrometers [54].

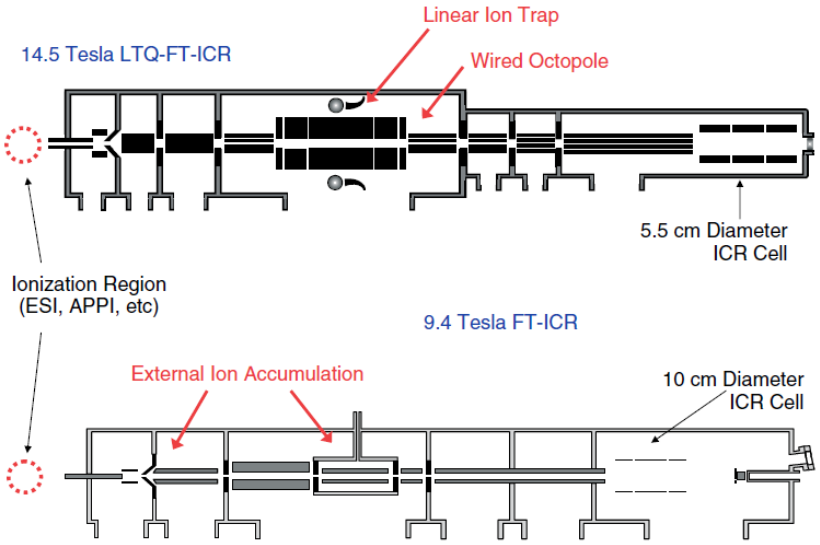

Figure 3-9. Configuration of FT-ICR mass spectrometers. Reproduced from [54]. Copyright 2011 John Wiley and Sons.

FT-ICR MS yields a very high resolution mass spectrum. Figure 3-10 shows the mass spectra obtained for Chinese and South American crude oils [54]. Figure 3-11 shows a zoomed in portion of the two mass spectra to demonstrate the high resolution obtained by the technique[54]. The horizontal axes on both figures show the mass to charge ratio (m/z). All ions are singly charged so the horizontal axis is equivalent to atomic mass units (Da)[53]. It is possible to detect very small differences in composition and distinguish between species that differ by a mass of 3 mDa or less [56].

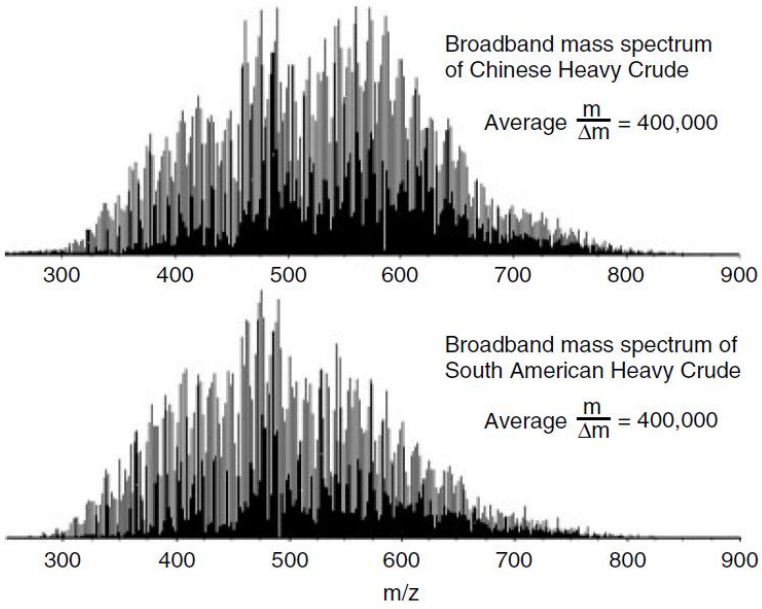

Figure 3-10. FT-ICR mass spectra for Chinese and South American crude oils. Reproduced from [54]. Copyright 2011 John Wiley and Sons.

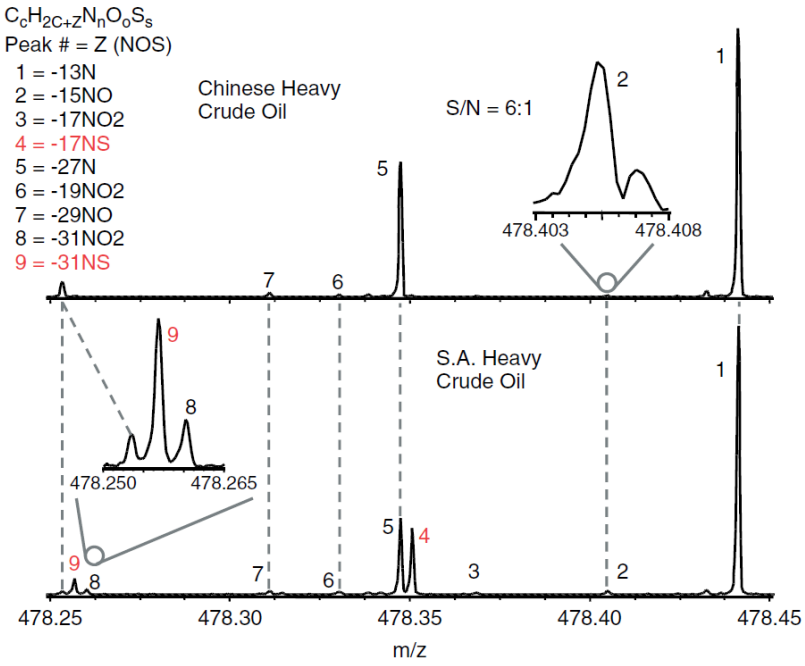

Figure 3-11. Zoomed in mass spectra for Chinese and South American crude oils. The axis shows mass to charge, but the ions are singly charged so the axis is equivalent to molecular weight. Reproduced from [54]. Copyright 2011 John Wiley and Sons.

Through analysis of the spectral data, the different heteroatom classes and their relative abundance can be determined. The accurate mass measurement can be combined with

the fact that petroleum and derivatives consist of homologous series. Each homologous series is categorized by heteroatom class ($N_nO_oS_s$), double bond equivalents (DBE) and carbon number [57]. DBE is a measure of aromaticity and calculated for compounds of the type $C_cH_hN_nO_oS_s$ using the equation:

DBE = c – h/2 + n/2 +1

If a homologous series of molecules are in the same heteroatom class and have the same DBE, then different members of that series will differ by units of $–CH_2$[57]. This difference equates to a difference in mass of 14.065 Da. Such a series can be easily identified if the Système international d'unités (SI) masses are converted to Kendrick masses using the equation:

Kendrick mass = SI mass x (14.00000/14.065)

This causes each member of the homologous series to differ by a Kendrick mass of 14.00000, thus having the same Kendrick mass defect[57]. Kendrick mass defect is defined by the equation:

Kendrick mass defect = nominal Kendrick mass – Kendrick mass

where the nominal Kendrick mass is the Kendrick mass rounded to the nearest integer. All compounds in the same alkylation series can be identified and assigned chemical formulas[57]. This process is carried out for the entire mass spectrum and can be presented a heteroatom class distribution[57]. Figure 3-12 shows an example of a heteroatom class distribution obtained from FT-ICR MS. The figure compares the heteroatom classes in distillation cuts for Middle Eastern heavy crude. [58]

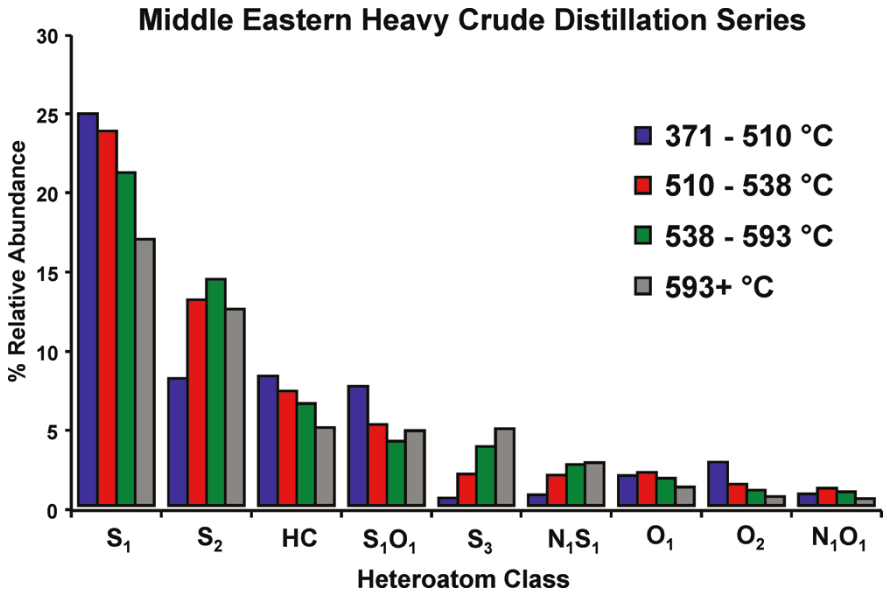

Figure 3-12. Heteroatom class distribution for distillation cuts of Middle Eastern heavy crude. Reprinted with permission from [58]. Copyright 2010 American Chemical Society.

In addition to the heteroatom class distribution, FT-ICR MS also allows for a detailed analysis of a single heteroatom class[57]. All of the compounds present within a given heteroatom class are typically plotted against their hydrogen to carbon ratio or their double bond equivalent. Both are measures of saturation. Figure 3-13 shows a comparison of the S_1 heteroatom class for different distillation cuts of Athabasca bitumen heavy vacuum gas oil. These are all of the molecules detected that contain a single sulfur atom. In these plots double bond equivalent is plotted against carbon number. [56]

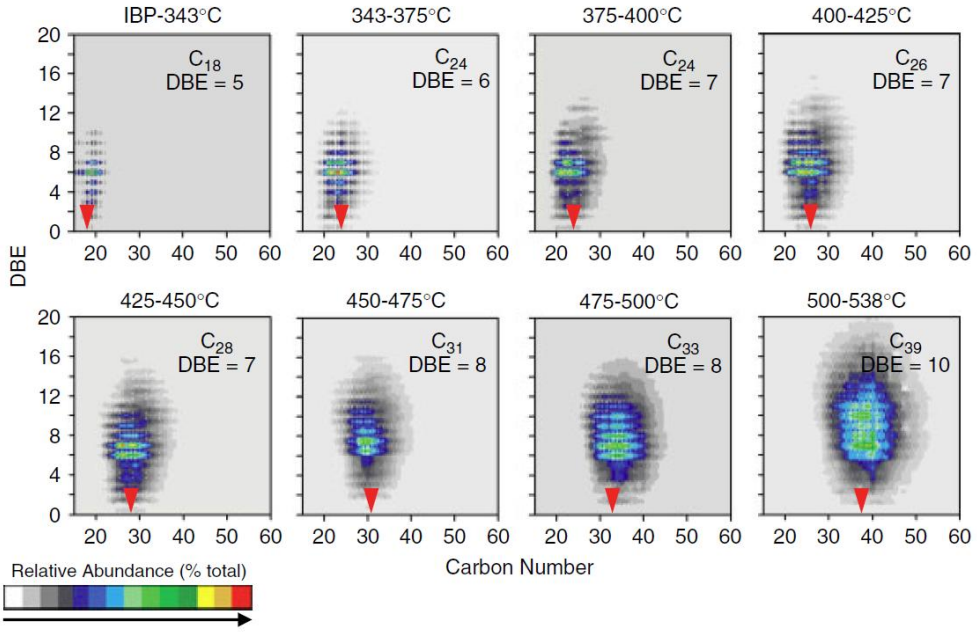

Figure 3-13. Comparison of S_1 heteroatom class for various Athabasca bitumen heavy vacuum gas oil cuts. Double bond equivalent is plotted against the carbon number. Reprinted with permission from [56]. Copyright 2010 American Chemical Society.

The type of data presented in the previous four figures is typically what to expect from FT-ICR MS experiments.

It is important to note the limitations of FT-ICR MS. The technique does not provide a mass balance in the analysis. It only allows for species to be counted. It gives relative abundance of heteroatom classes and abundance of species types within a heteroatom class, but this does not allow for determination of mass fractions of species present. As such, the measurements provide a detailed qualitative analysis of samples. Placing the samples in the composition space allows for comparison between samples, but cannot be used for the determination of exact composition.

The enriched sample was prepared using the previously described solvent extraction method. The entire beaker with the solid film was sent to the National High Magnetic Field Laboratory at Florida State University to minimize possibility of contaminants being introduced to the sample. Once the sample was received, it was extracted with toluene into a glass vial with a Teflon-lined cap. The solvent was evaporated in dry nitrogen and the sample was weighed. It was then dissolved in toluene (used as a solvent/dopant) to a concentration of 250 μg/mL in preparation for the APPI FT-ICR MS analysis.

A custom built adapter interfaced the APPI source (ThermoFisher Scientific, San Jose, CA) to the front stage of a custom built 9.4 T FT-ICR mass spectrometer[40]. The sample flowed through a fused silica capillary at a rate of 50 μL/min into a heated vaporizer chamber where nebulisation occurred with N_2 gas at 300°C. The sample then passed under a vacuum ultraviolet krypton gas discharge lamp (10 eV photons, 120 nm) where photoionization occurred. Ions were then swept into the first pumping stage of the mass spectrometer through a heated metal capillary inlet.

The equipment used was a positive ion APPI FT-ICR MS at 9.4 Tesla described in detail in[53]. Only liquid crystal enriched samples were analyzed using this technique, as related asphaltene and oil samples were analyzed during previous studies.

4. Results

Polarized Light Microscopy

The optical behaviour of C5 asphaltenes was examined from room temperature up to 200°C. As the temperature is increased liquid crystals form. The samples then become isotropic at high temperature. Once a sample becomes isotropic, liquid crystals do not reform on cooling. They also do not reform upon reheating after returning to room temperature. Thus the phase transitions appear to be irreversible. If liquid crystals are cooled to room temperature, they retain their order. If an isotropic sample is crushed using a spatula on a microscope slide (small amount of sample) or using a mortar and pestle (large amount of sample), the crushed material forms liquid crystals on reheating. In this respect a crushed sample is indistinguishable from a fresh sample. Crushing appears to "reset" the liquid crystal forming behaviour. Figure 4-1 shows each of the states and how they are achieved. All of the samples examined show the same type of behaviour, but possess different transition temperatures.

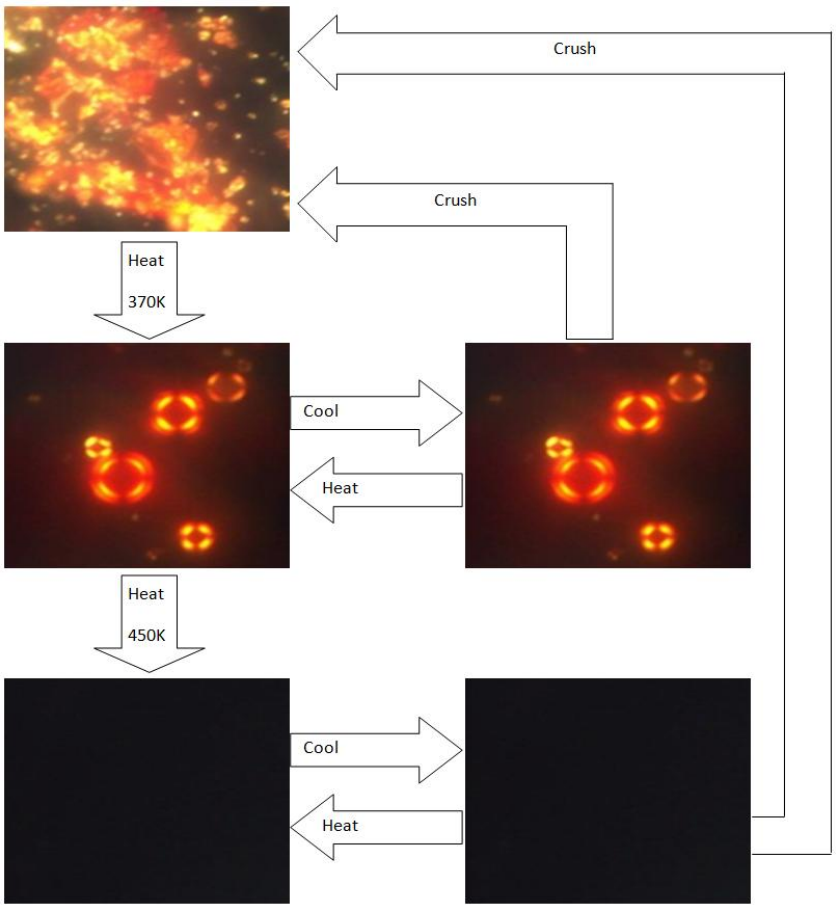

Figure 4-1. Crystalline states of Athabasca bitumen C5 asphaltenes. Top: solid. Middle: liquid crystal. Bottom: isotropic liquid.

Examining the appearance of the liquid crystalline state allows for a comparison between different samples. Figure 4-2 shows a visual comparison between C5 asphaltenes, SFE6, the liquid crystal enriched sample extracted from C5 asphaltenes, and the liquid crystal depleted sample following solvent treatment. Prior to extraction, the C5 asphaltenes has the lowest liquid crystal fraction. The liquid crystalline regions are small, only 10 µm in diameter, and sparse. SFE6 has larger liquid crystal regions than the asphaltenes - from 50 to 120 µm in diameter. For the liquid crystal enriched sample, the liquid crystals are not as large as those in the SFE6 sample, but they appear to comprise larger fraction of the sample over all. When the liquid crystal depleted material that remained on the slide after solvent treatment was crushed and reheated, it showed smaller liquid crystalline domains than the C5 asphaltenes sample and much less liquid crystal material than the enrich sample possessed prior to extraction.

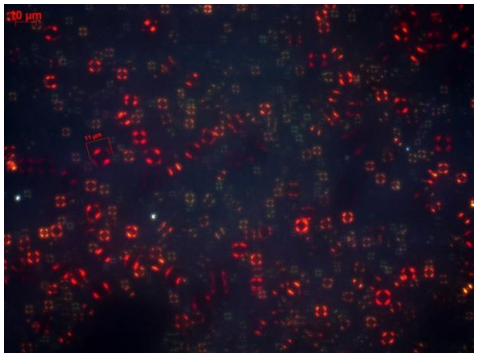

(a)

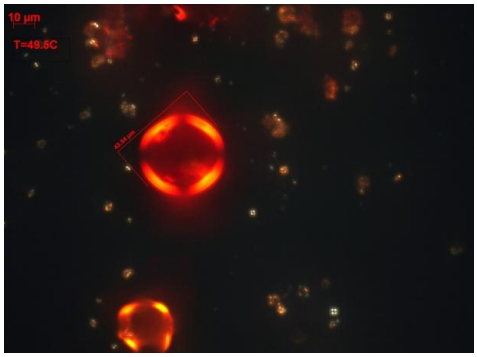

(b)

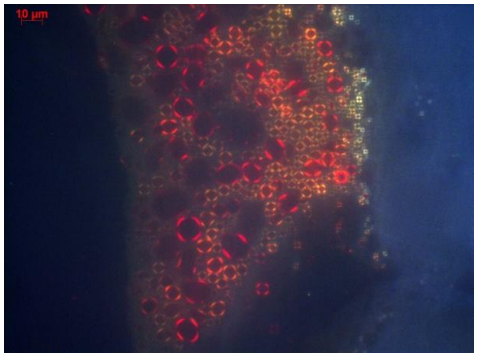

(c)

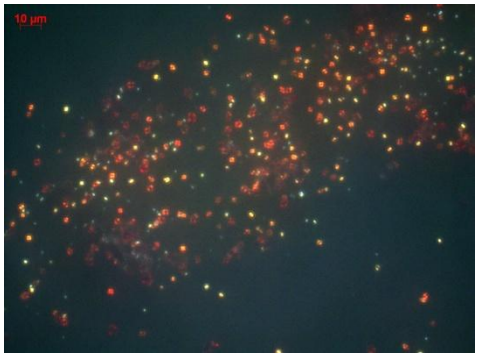

(d)

Figure 4-2. Comparison of liquid crystals in (a) C5 asphaltenes, (b) SFE6, (c) enriched liquid crystal sample extracted from C5 asphaltenes, (d) post extraction liquid crystal enriched sample.

Liquid crystals were also observed in C5 maltenes. In order for the behaviour to be exhibited, cooled maltenes had to be crushed. Ice crystals formed on some portions of the sample, but those regions were avoided during observation. As the maltenes were heated and melted, liquid crystals with diameters of approximately 30 µm in diameter were observed. The transition temperature of the liquid crystals in maltenes could not be determined due to the method used to observe them. The rapid freezing with liquid nitrogen and immediate reheating did not allow for accurate temperature measurement. Figure 4-3 shows the liquid crystalline behaviour of C5 maltenes. Liquid crystals were not observed if the sample was not crushed while frozen.

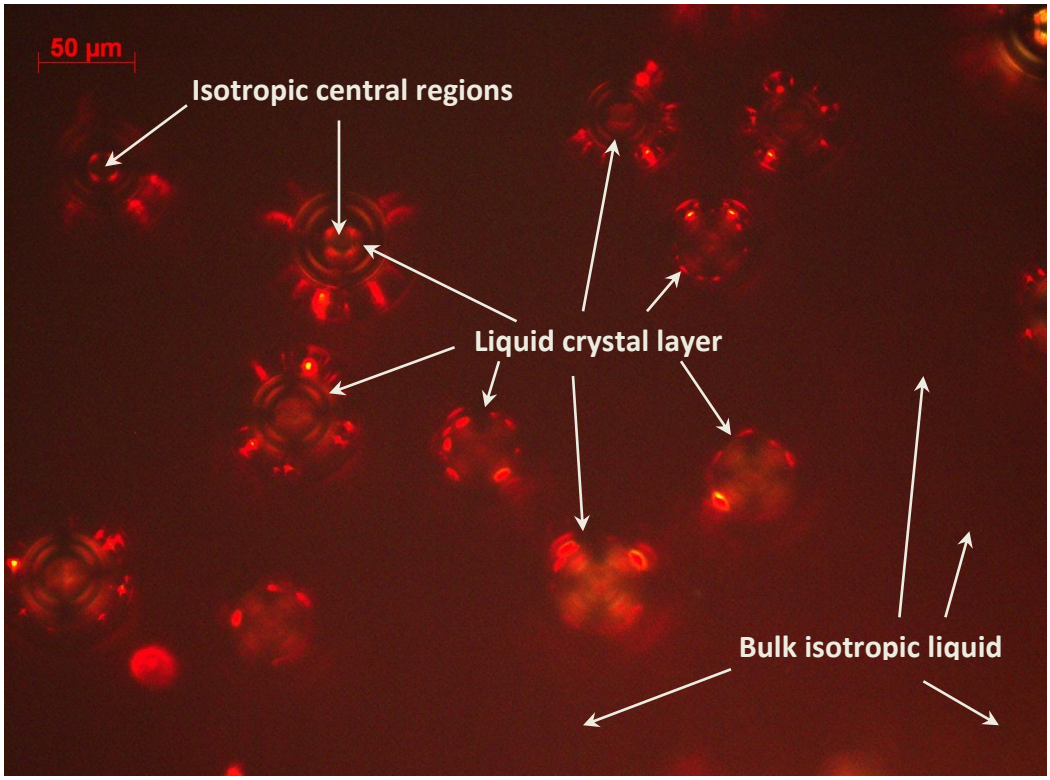

Figure 4-3. Liquid crystals observed in C5 maltenes. The liquid crystals that include an isotropic central region are suspended in a bulk isotropic liquid.

When liquid crystals from asphaltenes or SFE6 were observed in profile, a bright ring was observed to surround a dark central core. This observation is illustrated in Figure 4-4 for SFE6.

Figure 4-4. Profile view of a liquid crystal in SFE6.

By contrast, the model liquid crystal ($C_{21}H_{27}NO_2S$) showed reversibility in its phase transitions. The liquid crystalline behaviour was exhibited both upon heating and cooling. Figure 4-5 shows an image of $C_{21}H_{27}NO_2S$ in a nematic liquid crystal state.

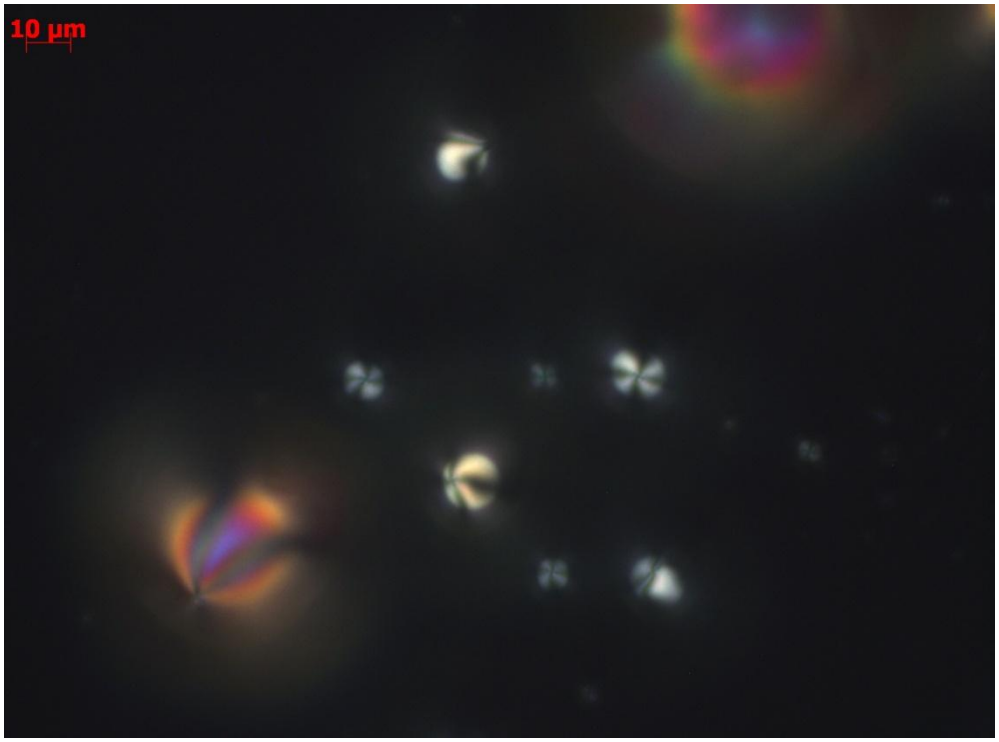

Figure 4-5. $C_{21}H_{27}NO_2S$ under cross polarized microscope. Nematic liquid crystal texture is observed.

Differential Scanning Calorimetry

To establish a baseline for comparison, DSC analysis was performed on a sample of $C_{21}H_{27}NO_2S$. Figure 4-6 shows the temperature dependence of the apparent specific heat capacity obtained. There is a large endothermic peak at 350.27 K associated with

an “anisotropic crystal to liquid crystal” transition with an enthalpy of 55.40 J/g and a smaller endothermic peak at 388.04 K corresponding to melting of liquid crystals with an enthalpy of 2.71 J/g. These transitions are real as the minimum detectable transition enthalpy by DSC is on the order of 0.1 J/g. The transition temperatures and anisotropic to liquid crystal enthalpy agree with what has been reported [59] but the liquid crystal melting enthalpy was not reported there. The enthalpy of the liquid crystals melting is on par with what has been reported for other similar liquid crystal compounds [60].

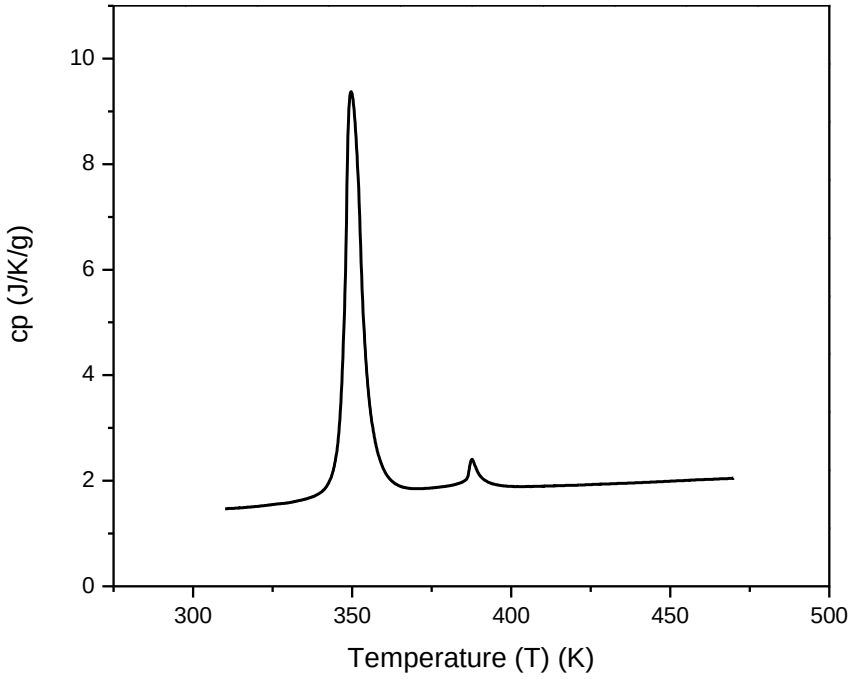

Figure 4-6. Temperature dependence of the apparent specific heat capacity for 4-Isothiocyanatophenyl 4-pentylbicyclo[2,2,2]octane-1-carboxylate.

The liquid crystalline behaviour of asphaltenes is also seen in DSC analysis. Figure 4-7 shows the temperature dependence of the apparent specific heat capacity for C5 asphaltenes. There is a small endothermic peak at 370 K. There is a broad exothermic region from 400 to 450 K as well as a broad endotherm that ranges from approximately 320 K to 520 K corresponding to isotropic melting. These peaks are only present on the first run. On the second run the complex peaks are replaced by a single glass transition that occurs over the same temperature range. This behaviour agrees with what has been reported elsewhere [61].

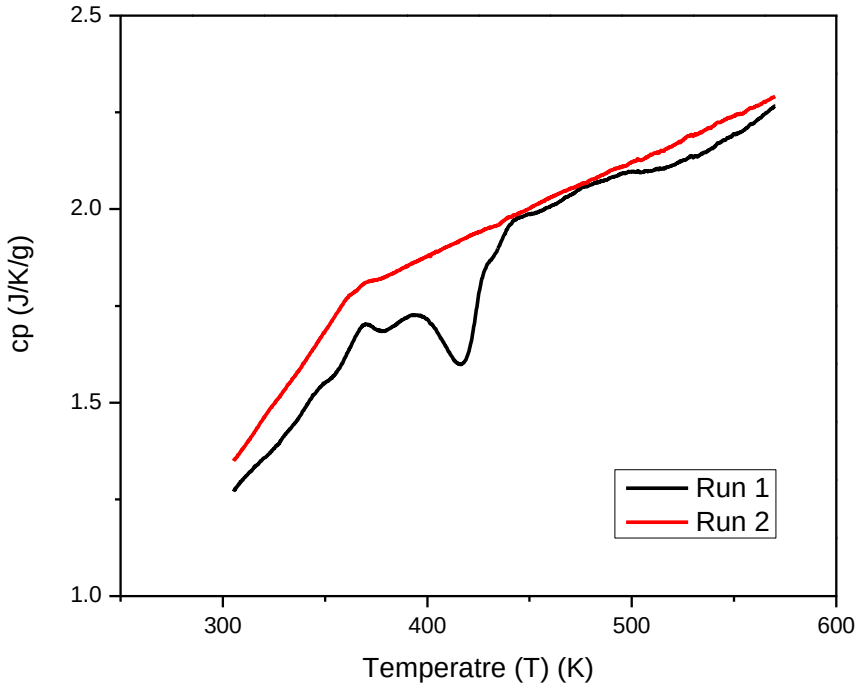

Figure 4-7. Temperature dependence of the apparent specific heat capacity for C5 asphaltenes.

DSC was also performed on a sample of C5 asphaltenes that had been heated and then crushed. Figure 4-8 shows the temperature dependence of the apparent heat capacity for the heat treated and crushed asphaltenes. The same peaks are observed as in fresh C5 asphaltenes, but they are not as pronounced. The peaks are not present on subsequent heating cycles.

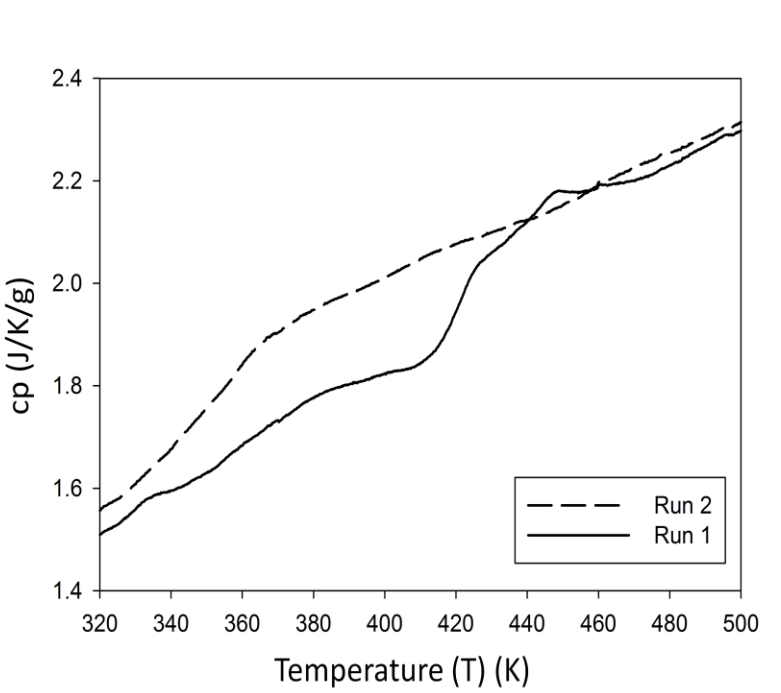

Figure 4-8. Temperature dependence of the apparent heat capacity for C5 asphaltenes that were heat treated and crushed.

The SFE6 fraction was also examined by DSC. Figure 4-9 shows the temperature dependence of specific heat capacity for SFE6. There is a glass transition followed by two endothermic peaks - at 320 K and 370 K. The same peaks were not observed on subsequent heating cycles.

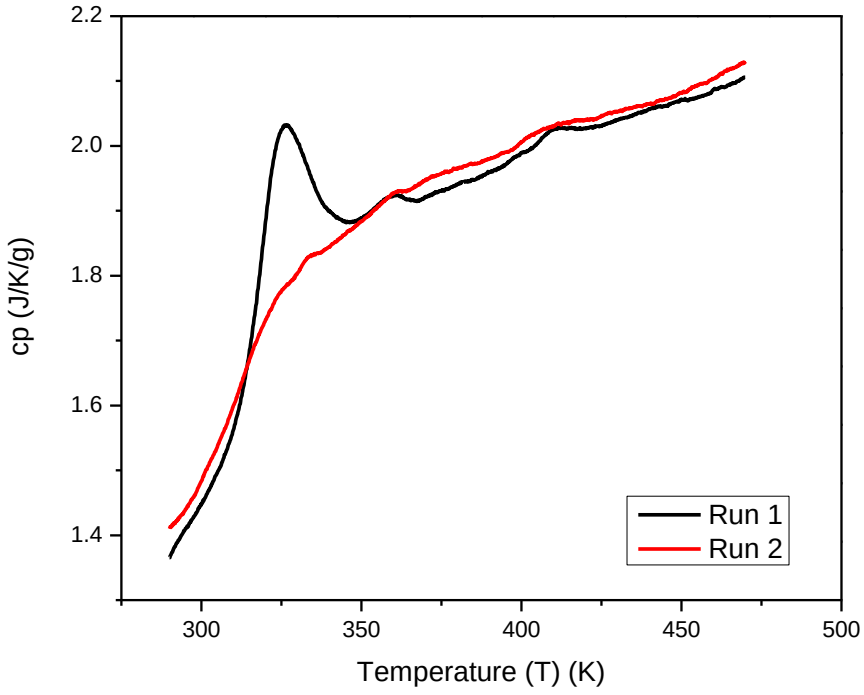

Figure 4-9. Temperature dependence of apparent specific heat capacity for SFE6 during successive heating cycles.

Photoacoustic Infrared Spectroscopy

The results above suggest that the liquid crystals are biplex. That is, there are two distinct regions present: an isotropic region and an anisotropic region. In principle depth profiling and surface based PA-IR measurements permit observation co-existing materials within samples and the impact of heat or other treatments on the distribution of materials. Depth profiling allows for the analysis of different layers within a sample and can determine where the liquid crystals are. Standard PA-IR examines the surface layer of a sample and provides a means of comparison between samples that have been treated in various ways. Both of these methods have been used and are presented here.

Depth profiling

A thin layer of powdered SFE6 was spread on a piece of aluminum and heat treated so that liquid crystals formed. Depth profiling was then performed by Dr. Qing Wen at CANMET on the sample and the results compared with asphaltene and with SFE6 samples that were not heat treated. As the aromatic carbon content was expected to vary significantly among the the three materials, the aromatic carbon fraction was used to trace composition variation. The results are shown in Figure 4-10. The asphaltenes

have the highest proportion of aromatic C-H and the SFE6 lowest aromatic C-H overall while the liquid crystals have a proportion of aromatic C-H between the asphaltenes and SFE6. At the surface all three samples appear to have approximately the same proportion of aromatic C-H. As the liquid crystals are probed more deeply, their aromatic C-H fraction approaches that of a bulk SFE6 sample from which they were formed. The error bars are obtained using the standard deviation of three measurements.

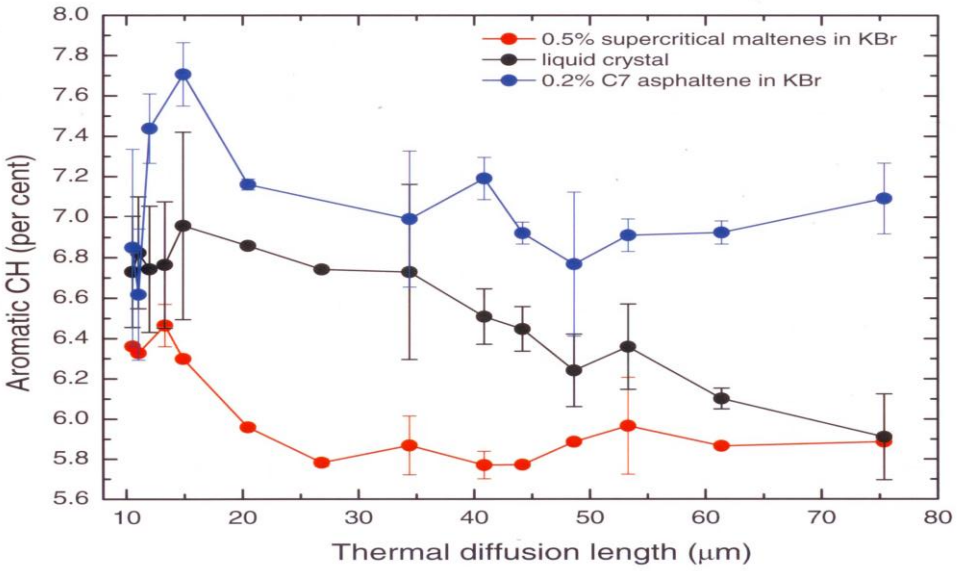

Figure 4-10. Results of depth profiling. Aromatic C-H as a percentage of total C-H stretching region plotted against thermal diffusion length. The black points are for liquid crystal droplets formed from SFE6. The red points are for SFE6 in KBr. The blue points are for asphaltenes in KBr. Lines are added for visual purposes.

Standard PA-IR Measurements

Figure 4-11 shows the results for the 3050 cm^{-1} C-H band for C5 and C7 asphaltenes treated in the various ways listed in Table 3-2. C5 and C7 asphaltenes both show the same trends. The fresh and crushed samples give the same apparent aromaticity within the experimental error. Heat treating the sample causes the apparent aromaticity at the surface and to a depth of approximately 5 μm (based on the modulation frequency of 1.6 kHz) to decrease. While the error bars are large, crushing heat treated samples increases the as measured aromatic C-H content. This suggests the heat treated asphaltene surfaces are aromatic carbon deficient relative to the bulk asphaltenes. The error bars were obtained using the standard deviation of two measurements.

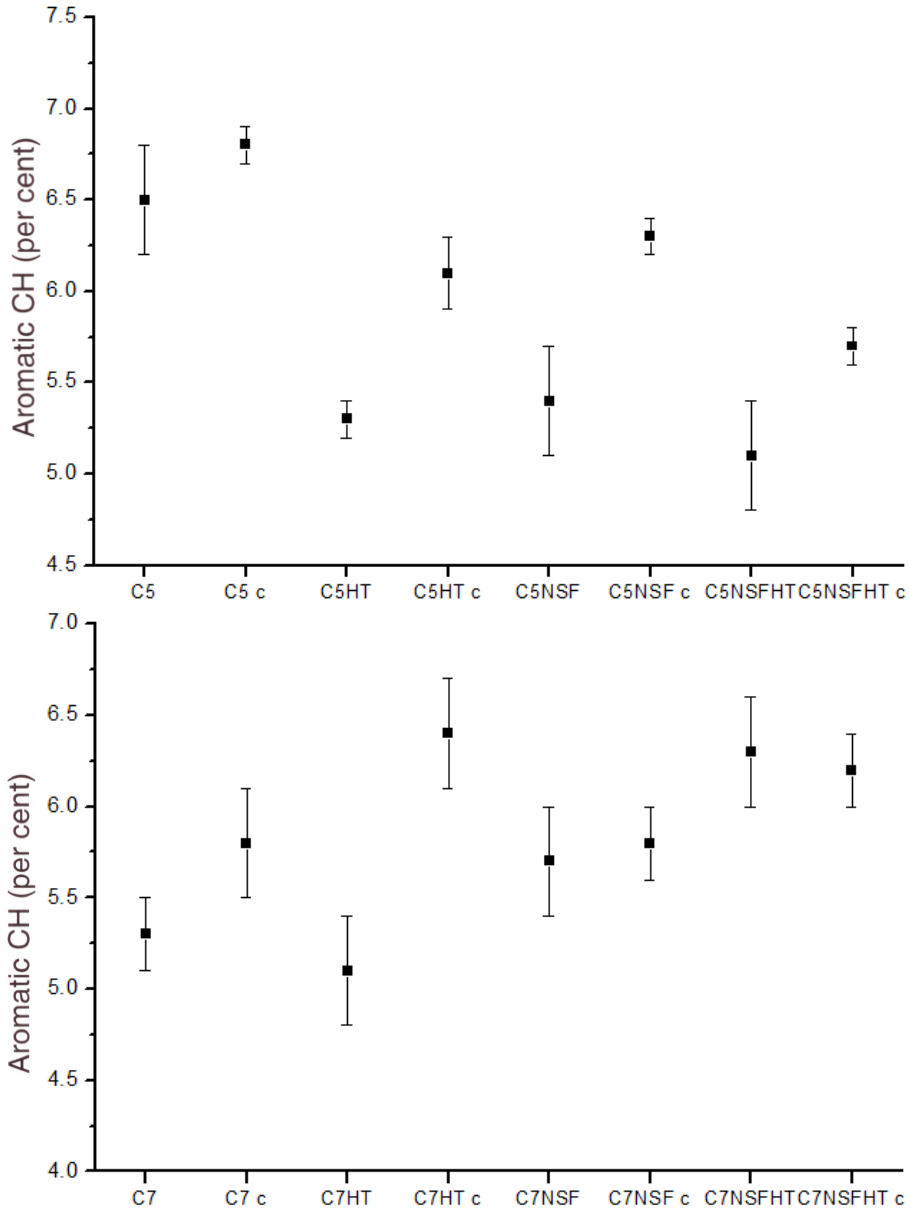

Figure 4-11. Results from PA-IR experiments for bulk analysis (top) C5 asphaltenes and (bottom) C7 asphaltenes treated in various ways. Y-axis shows aromatic C-H stretching (3000 – 3100 cm^{-1}) as a percentage of the total C-H stretching region (2760 – 3100 cm^{-1}).

Fourier Transform Ion Cyclotron Resonance Mass Spectrometry

The liquid crystal enriched sample extracted from Athabasca C5 asphaltenes was analyzed using APPI FT-ICR MS at 9.4 T by Amy McKenna at the NHMF laboratory at Florida State University Tallahassee. Figure 4-12 shows the mass spectrum that was obtained.

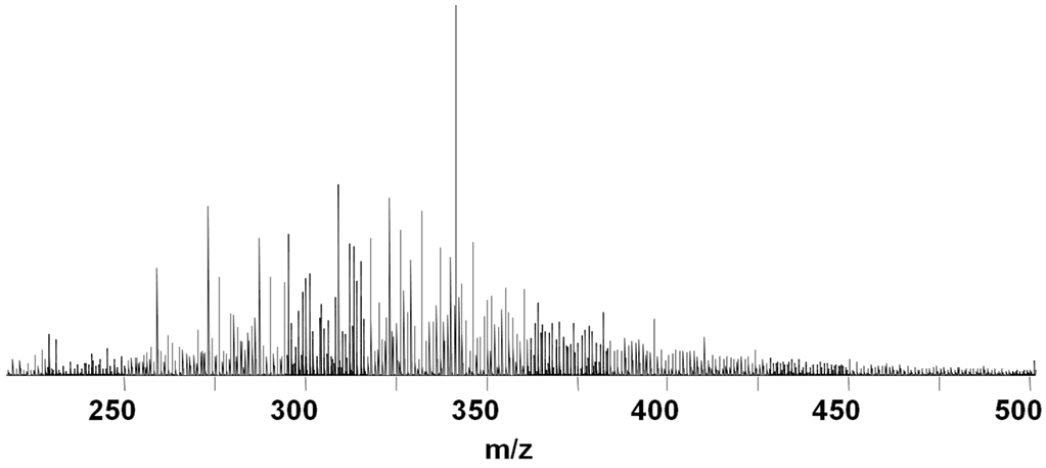

Figure 4-12. Mass spectrum for liquid crystal enriched sample. There are 26086 peaks at 200 < m/z < 500.

Figure 4-13 shows the heteroatom class distribution for the liquid crystal enriched sample. The top four heteroatom groups are sulphur, hydrocarbon, nitrogen and oxygen.

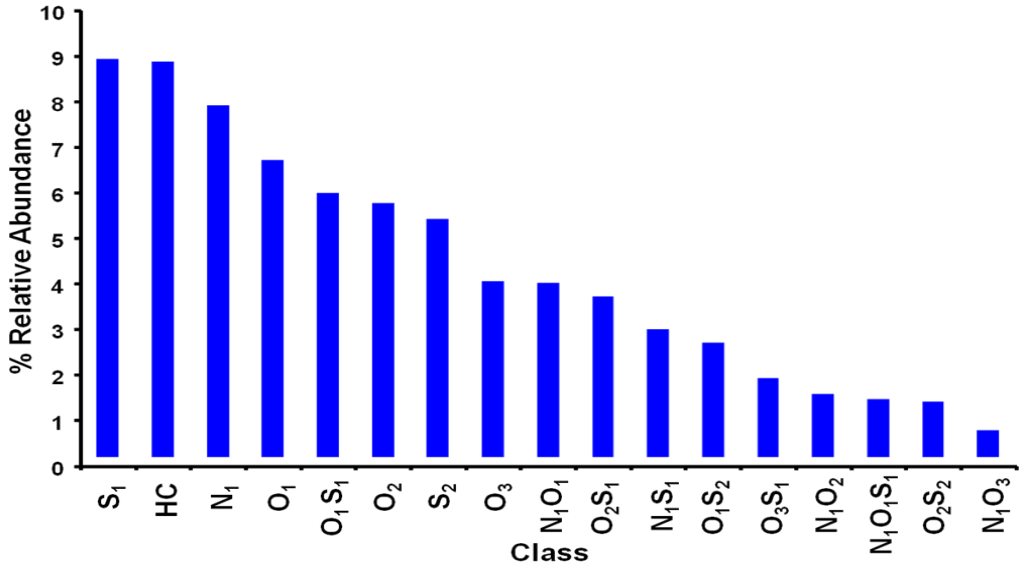

Figure 4-13. Heteroatom abundance distribution for liquid crystal enriched sample for the 17 most abundant classes.

Figures 4-14 through 4-21 show the hydrogen to carbon ratio and double bond equivalents plotted against the carbon number for selected heteroatom classes for the liquid crystal enriched sample. The plots are for the combined odd and even electron positive ions.

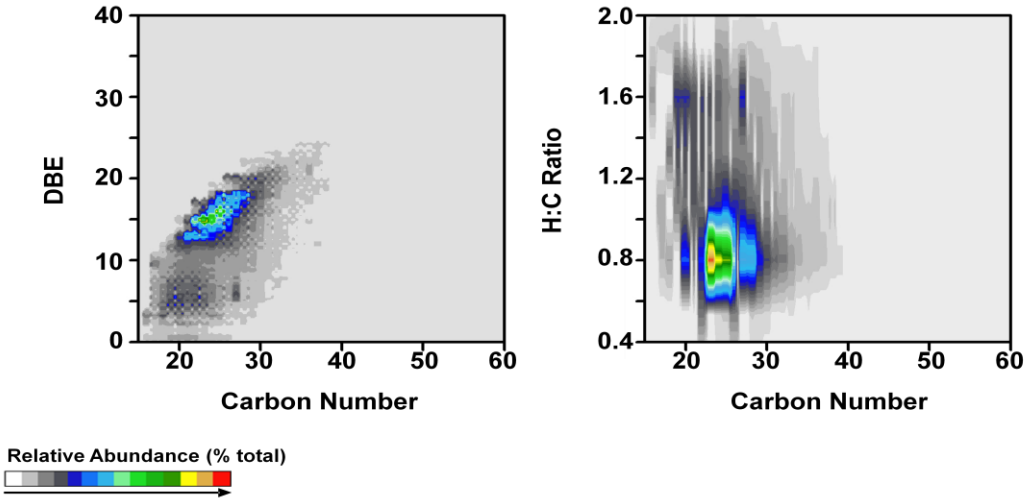

Figure 4-14. Double bond equivalent and hydrogen to carbon ratio plots for hydrocarbon class for the liquid crystal enriched sample.

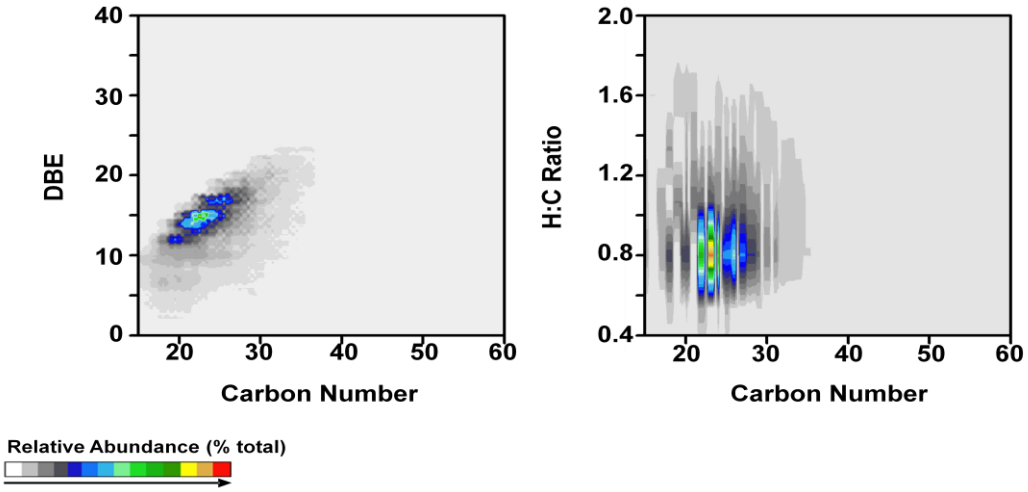

Figure 4-15. Double bond equivalent and hydrogen to carbon ratio plots for S_1 class for the liquid crystal enriched sample.

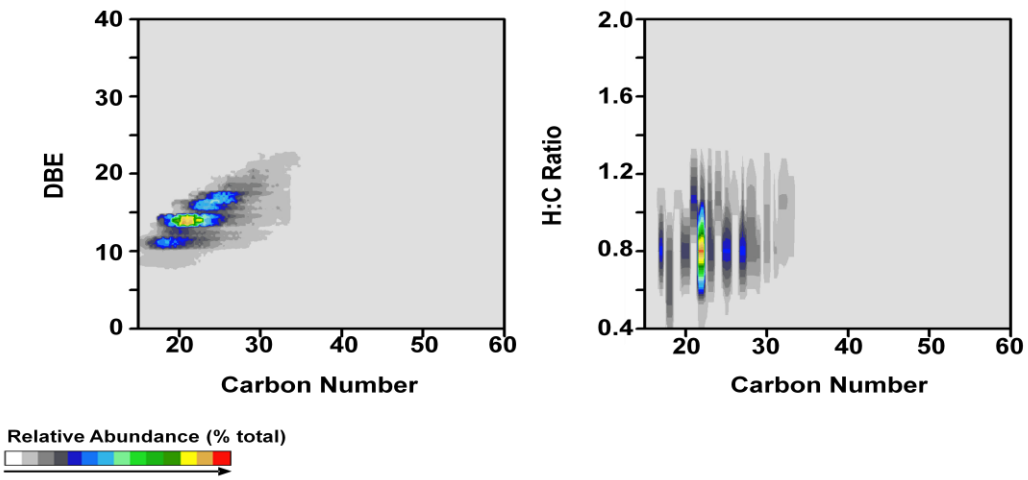

Figure 4-16. Double bond equivalent and hydrogen to carbon ratio plots for S_2 class for the liquid crystal enriched sample.

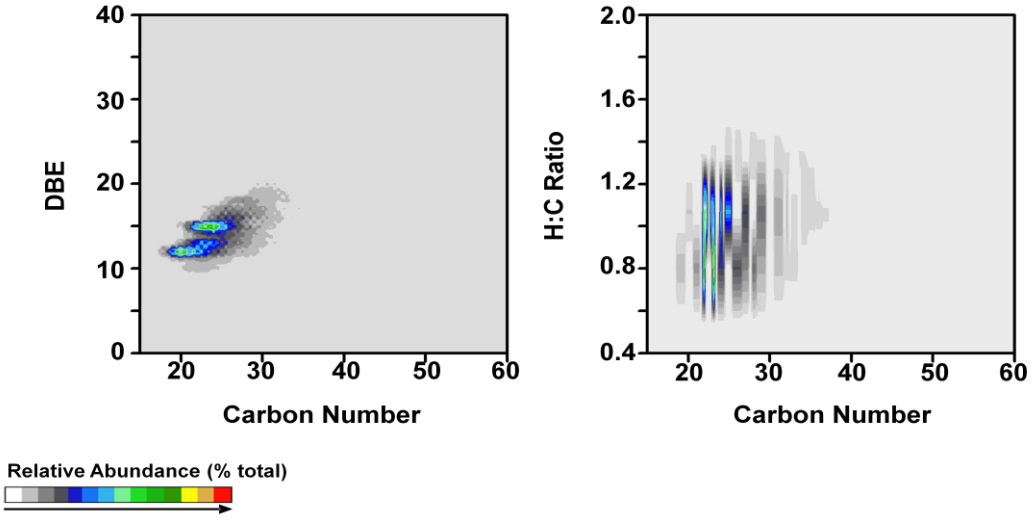

Figure 4-17. Double bond equivalent and hydrogen to carbon ratio plots for N_1 class for the liquid crystal enriched sample.

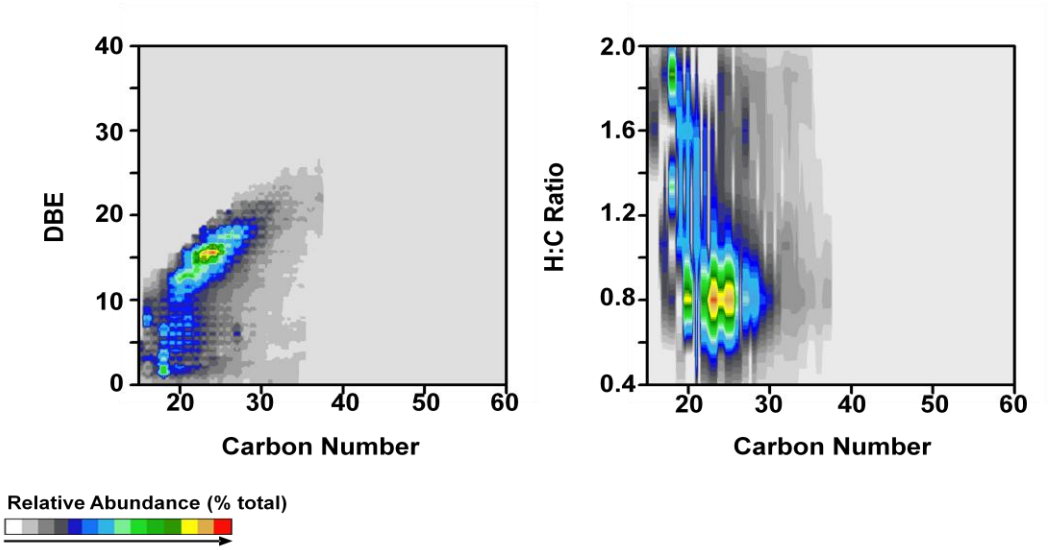

Figure 4-18. Double bond equivalent and hydrogen to carbon ratio plots for O_1 class for the liquid crystal enriched sample.

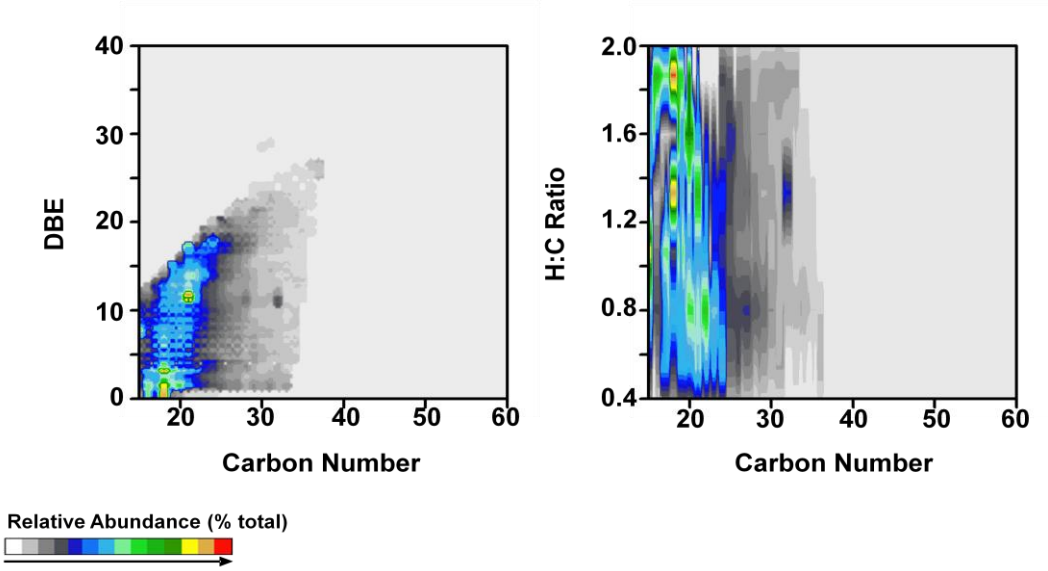

Figure 4-19. Double bond equivalent and hydrogen to carbon ratio plots for O_2 class for the liquid crystal enriched sample.

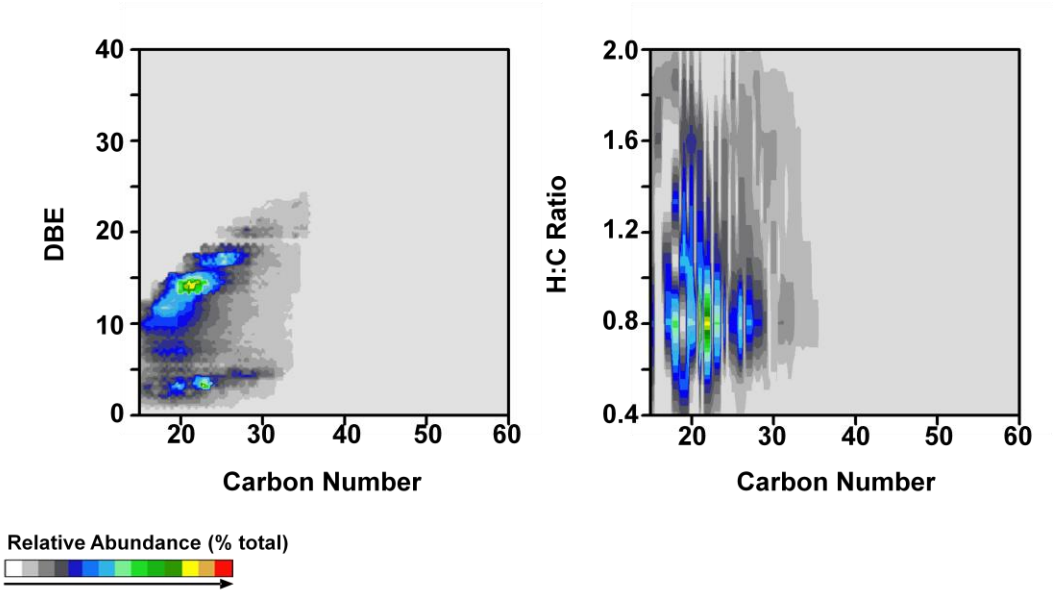

Figure 4-20. Double bond equivalent and hydrogen to carbon ratio plots for SO class for the liquid crystal enriched sample.

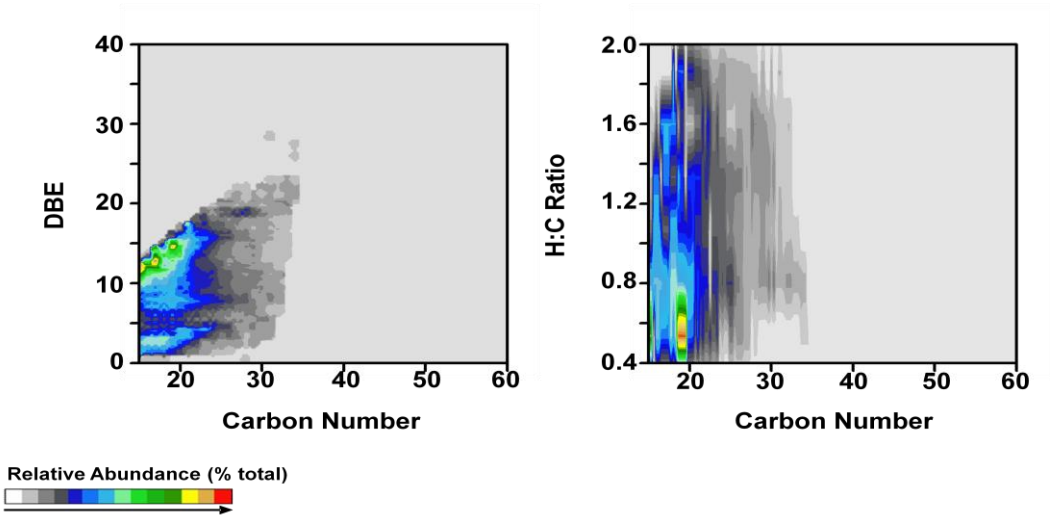

Figure 4-21. Double bond equivalent and hydrogen to carbon ratio plots for SO_2 class for the liquid crystal enriched sample.

5. Discussion

Overview

In this chapter, the results presented in Chapter 4 are discussed relative to one another and the relevant literature presented in Chapter 2.

Liquid Crystal Physical Properties

Polarized Light Microscopy

Liquid crystals were observed in all fractions of petroleum investigated. Such observations allow for the evaluation of the relative quantity of liquid crystalline material present in each fraction. This evaluation is subjective, but significant differences are readily identified. The diameter and number of the domains were used to decide the relative quantity of the liquid crystals. Further, only liquid crystals on or adjacent to the surface of slides were counted. The relative fractions of liquid crystalline material are: enriched sample extracted from Athabasca bitumen C5 asphaltenes > SFE6 > C5 asphaltenes. The absolute mass/volume fractions were not determined. Athabasca bitumen pentane maltenes also had liquid crystals present, but it was difficult to judge the relative fraction because the transitions to liquid crystal and isotropic liquid arose below room temperature under conditions where temperature could not be controlled with the available apparatus. The transitions occurred as the sample heated rapidly from approximately the boiling point of nitrogen (77 K) to room temperature in the microscope.

It is evident from the behaviour observed in the microscope that the liquid crystal domains comprised two phases: an isotropic core surrounded by a liquid crystalline layer. In asphaltene samples these domains formed primarily on the surface of the microscope slides, while in the C5 maltenes and in the liquid crystal enriched sample extracted from C5 asphaltenes, liquid crystals were primarily suspended in isotropic liquid.

While, the circular pattern with the dark cross observed is similar to the smectic texture shown in Figure 3-2, this does not necessarily mean that the petroleum liquid crystals are smectic. The presence of an isotropic core in addition to the liquid crystal layer is fundamentally different from the pure liquid crystals described in the literature and complicates the interpretation. The optical similarity though is suggestive and permits a tentative assignment of the liquid crystals as smectic, i.e.: the molecular ordering is one-dimensional and similar to the stacking pattern in smectic liquid crystals as illustrated in Figure 2-1.

Polarized Light Microscopy and Depth Profiling

The biplex nature of the petroleum liquid crystals was further corroborated by performing PA IR depth profiling experiments on liquid crystals within the SFE6 sample adhering to an aluminum substrate. The geometry is illustrated in Figure 5-1, where the black isotropic core is surrounded by a red anisotropic layer. Depth profiles were performed on multiple liquid crystal domains simultaneously because a single liquid crystalline region in SFE6 is in the range of 50 to 120 µm in diameter and has less area than the minimum 10 mm^2 required for PA-IR. The liquid crystalline domains are approximately hemispherical – Figure 4.4. The thickness of the liquid crystal layer is at most 35 µm but likely closer to 15 µm when these results are compared with microscopy. 15 µm is where the aromatic C-H first begins to decrease in the depth profiles. Depth profiles were performed to a depth of 75 µm. Cartoons of the geometry are superimposed on the SFE6 depth profile results reported in Figure 4-9, in Figure 5-2. With the cartoon, the interpretation of the results is clear. The upper surface is dominated by liquid crystal rich material which is intermediate between SFE6 and asphaltenes in nature. With increasing depth, the material gradually approaches the composition of the bulk SFE6 material from which the liquid crystals are derived. To a first approximation, the isotropic core comprises SFE6 material. For asphaltenes, a similar physical structure is observed. The liquid crystals appear on outer surfaces of asphaltene particles.

The combination of cross polarized light microscopy and depth profiling suggests that materials capable of forming liquid crystals are present as a separate phase on the exterior surfaces of drops or particles of petroleum fractions, or migrate to exterior surfaces of drops or particles on heating to form a separate phase. Another phase remains isotropic at the centre of drops or particles.

Depth profiling and optical microscopy allow for measurement of the particle dimensions and therefore a rough estimation of the volume fraction of liquid crystal material. If the droplet is assumed to be a perfect hemisphere with the liquid crystal layer having a thickness of 15 µm, this yields a volume fraction of 65%. This is far greater than the yield of enriched sample obtained using solvent extraction. This discrepancy is due to a combination of effects. Microscopy and depth profiling have likely overestimated the thickness of the liquid crystal layer. It is also likely that the extraction did not remove all of the liquid crystals from the original sample – only a portion of the exterior layer. This result suggests that a multi-stage extraction could be successful in creating more enriched liquid crystal samples.

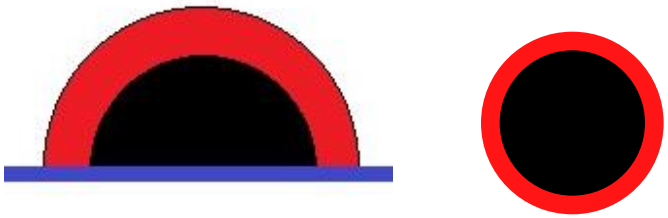

Figure 5-1. Left: Cross-sectional view of a liquid crystal domain on a surface. Right: Bottom-up/top-down view of a liquid crystal domain on a surface.

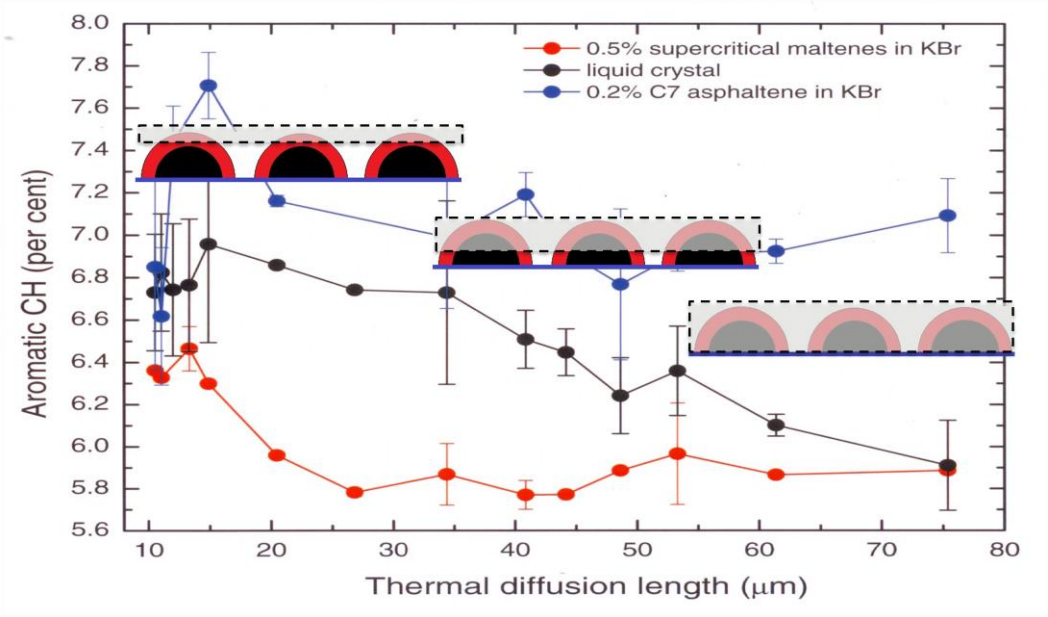

Figure 5-2. Details of depth profiling liquid crystal droplets formed from SFE6 compared with SFE6 in KBr and C7 asphaltenes in KBr. The highlighted portion shows what is being scanned at each depth for the SFE6 liquid crystals.

Photoacoustic Infrared Spectroscopy

The composition differences observed in the survey of asphaltenes subject to various treatments and reported in Figure 4-11 suggests that materials capable of forming liquid crystals migrate to exterior surfaces on heating. For example, in Figure 4-11 a and b, the aromatic C-H relative abundance for as prepared and crushed C5 and C7 asphaltenes are comparable, while for their heat treated analogues, the differences are significant. As the PA-IR measurements only probe to a depth of 5 μm, the liquid crystal forming material must migrate to the surface during heating for these cases. By contrast, the C5 NSF samples possess distinct regions, even in the absence of thermal treatment, and this basic physical structure is not affected by heat treatment. Liquid crystals appear to form in place (at the surface of particles) on heating. C7 NSF samples are not readily distinguished on this basis.

Differential Scanning Calorimetry and Optical Microscopy

Peaks observed using DSC correspond to the formation and disappearance of liquid crystals. The endothermic peak at 370 K in Figure 4-7 corresponds to the formation of liquid crystals. The exothermic region from 400-450 K corresponds to the disappearance of the liquid crystals. The transition appears as exothermic because the liquid crystals dissolve into the isotropic core and the particles/drops become isotropic. Enthalpies of mixing are often negative and can swamp small phase transition enthalpies, if present [62, 63]. From the DSC curve for $C_{21}H_{27}NO_2S$, Figure 4-6, the enthalpy of transition for a pure crystalline solid to a pure liquid crystal, 55.40 J/g for this case, is much larger than the enthalpy of transition of a liquid crystal to a pure liquid, 2.71 J/g for this case.

As the endothermic peak at 320 K, in Figure 4-8, coinciding with the formation of liquid crystals in the SFE6 sample is much larger than the corresponding peaks for asphaltenes in Figure 4-7, the DSC results are consistent with the optical observations and provide a relative measure of liquid crystal forming material mass fraction in the various samples. The results also help explain why the enthalpy of transition from liquid crystal to liquid is exothermic for C5 asphaltenes (dissolution effects dominate at low mass fraction), endothermic for SFE6 (phase transition effects dominate at high mass fraction).

During the second heating cycle, a liquid crystalline phase transition is not observed optically and is not present in the heat capacity data for C5 asphaltenes as shown in Figure 4-7. Once the sample becomes isotropic, it no longer forms liquid crystals unless it is crushed between heating cycles as shown in Figure 4-8. A fresh sample is made up of many sub-micron sized particles. There is space for the liquid crystal material to move to the exterior surfaces as the sample is heated. When it completely melts and solidifies these exterior surfaces and tiny spaces no longer exist and the liquid crystals are unable to form before the entire sample melts again. Crushing disrupts the surfaces and provides fresh surfaces on which liquid crystals can form.

Chemical Analysis

Fourier Transform Ion Cyclotron Resonance Mass Spectrometry

The analysis performed using FT-ICR MS provided a lot of information about the liquid crystal enriched sample extracted from Athabasca bitumen C5 asphaltenes. The results from this analysis show that there is a profound difference between the composition of the liquid crystals and for example, Athabasca bitumen C7 asphaltenes. The liquid crystals can be considered a separate material from asphaltenes.

Figure 5-3 shows the FT-ICR mass spectrum for Athabasca C7 asphaltenes [40]. The spectrum ranges from m/z = 400 to m/z = 900, though there are smaller peaks outside of this range. The liquid crystals in this work were obtained from C5 asphaltenes, and a mass spectrum for C5 asphaltenes is unavailable for comparison. It is expected to be

similar to that of the C7 asphaltenes in Figure 5-3. When the mass spectrum for C7 asphaltenes is compared with the mass spectrum for the liquid crystals in Figure 4-13, it is evident that the liquid crystals come from the lightest portion of the asphaltenes.

Figure 5-4 shows the relative abundance distribution for heteroatom containing fractions for Athabasca C7 asphaltenes [40]. Comparable data for the liquid crystal enriched sample, Figure 4-13, suggest that the liquid crystal rich sample is enriched in sulphur, oxygen and nitrogen relative to asphaltenes. The extent of the enrichment cannot be quantified on the basis of these data, even though they were analyzed on the same device using the same configuration, because abundance does not correlate directly with mass fraction. Regrettably, too little sample could be prepared to perform an elemental analysis.

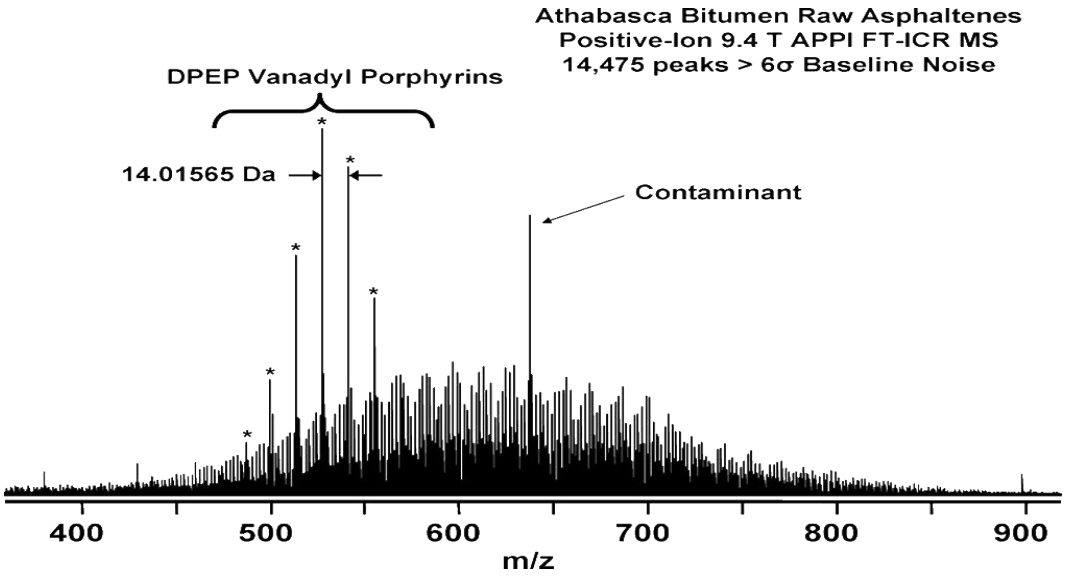

Figure 5-3. Mass spectrum for Athabasca C7 asphaltenes. The contaminant at m/z = 637 is unknown and is probably a result of the asphaltene fractionation process. Reprinted with permission from [40]. Copyright 2009 American Chemical Society.

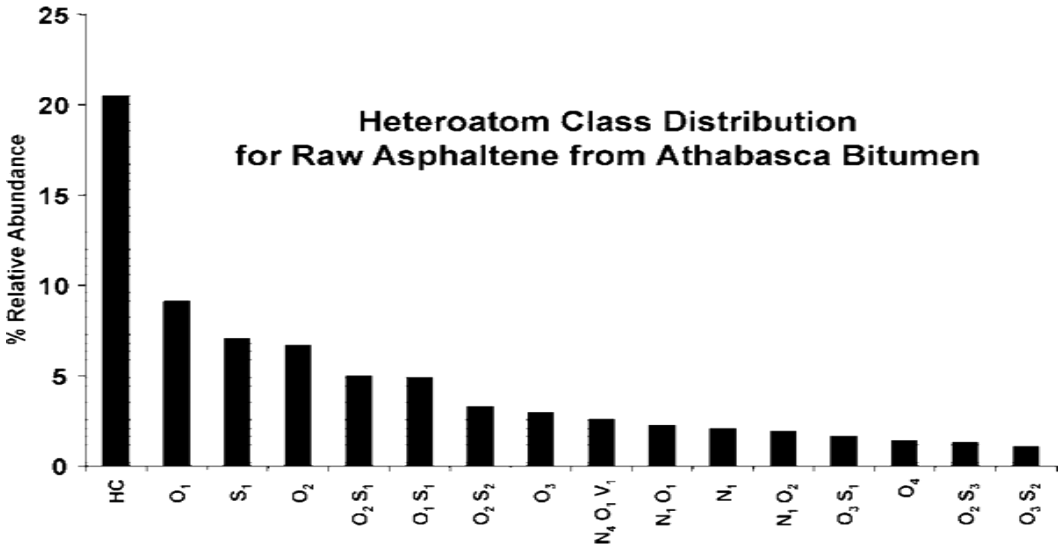

Figure 5-4. Heteroatom class distribution for Athabasca C7 asphaltenes for 16 most abundant classes. Reprinted with permission from [40]. Copyright 2009 American Chemical Society.

The only asphaltene heteroatom class available for comparison in the form of a DBE vs. carbon number plot was the O_2 class. Other heteroatom classes were not available in the literature for comparison. Figure 5-5 shows the DBE plotted against the carbon number for the Athabasca C7 asphaltenes O_2 class [40] with the red circle indicating where the O_2 class is for the liquid crystal enriched sample. The carbon number for the asphaltenes is much higher than for the enriched sample. This observation means that the molecules in the enriched sample are smaller and lighter than the bulk of the asphaltenes. In addition to the lower carbon number, the O_2 class in the liquid crystal enriched sample is also less aromatic. These differences suggest that the liquid crystals are formed from a material that is distinctly different from "bulk" asphaltenes.

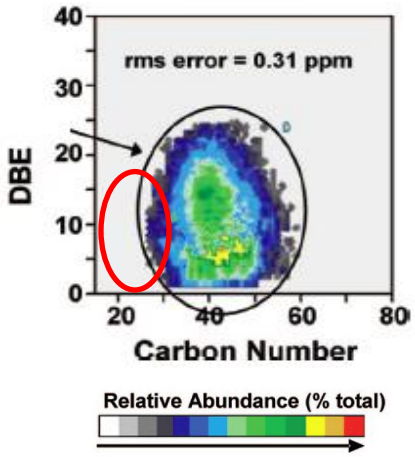

Figure 5-5. DBE vs carbon number plot for O_2 class in Athabasca C7 asphaltenes. The red circle highlights the area on the plot that the O_2 class for the liquid crystal enriched sample occupies. Adapted with permission from [40]. Copyright 2009 American Chemical Society.

The liquid crystal enriched sample can be compared to Athabasca bitumen heavy vacuum gas oil (HVGO) in order to place it in composition space [56]. The HVGO was fractionated using ASTM D-1160 and collected in eight 25°C intervals. Each fraction was analyzed individually using FT-ICR MS. Figure 5-6 shows the DBE vs carbon number plot for the HC class of Athabasca bitumen HVGO for all distillation cuts[56], with the area of the liquid crystal enriched sample circled. The liquid crystals are comparable in size and aromaticity to the lightest and most aromatic portion of the HVGO.

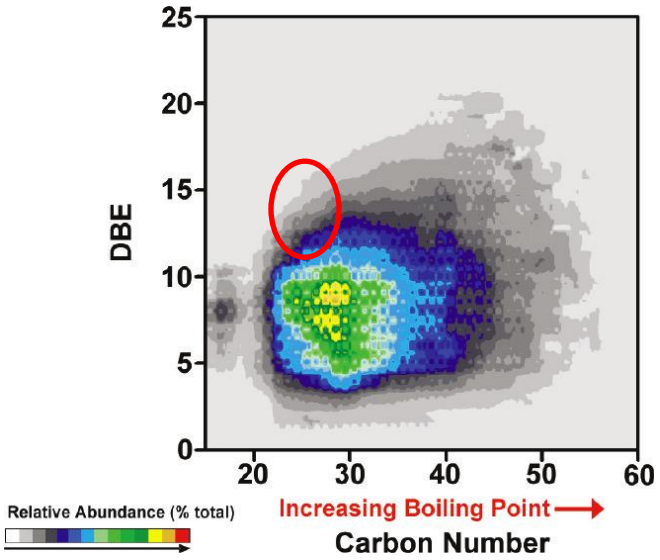

Figure 5-6. DBE vs carbon number plot for HC class of Athabasca bitumen HVGO for all distillation cuts. Circle highlights the area on the plot that the HC class of the liquid crystal enriched sample occupies. Adapted with permission from [56]. Copyright 2010 American Chemical Society.

Figure 5-7 shows the DBE vs carbon number plot for the S_1 class of Athabasca bitumen HVGO [56]. Again, the liquid crystal enriched sample is comparable to the smallest and most aromatic molecules. The liquid crystals are on the very edge of the detected compounds in HVGO. Through these observations it can be concluded that the liquid crystals come from the lightest portion of what is considered heavy oil.

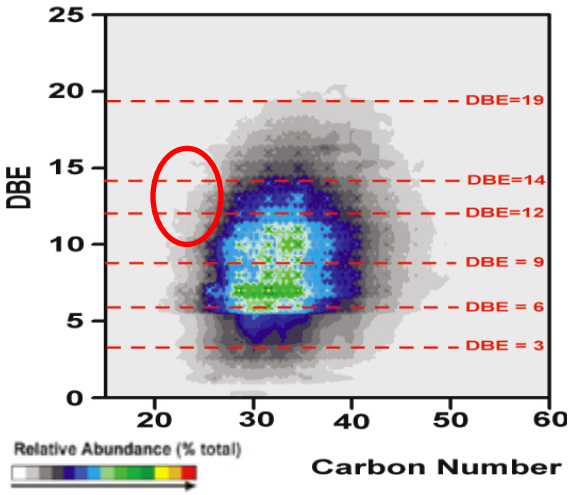

Figure 5-7. DBE vs Carbon number plot for S_1 class of Athabasca bitumen HVGO. The circle highlights the area on the plot that the S_1 class of the liquid crystal enriched sample occupies. Adapted with permission from [56]. Copyright 2010 American Chemical Society.

By contrast, the heteroatom class distribution in the liquid crystal enriched sample is similar to material extracted from a bitumen-water interface [32, 64], particularly materials collected below a critical dilution point. The interfacial material was analyzed using FT-ICR MS. The analysis in [64] used ESI instead of APPI for ionization so the comparison is not perfect. ESI cannot ionize nonpolar compounds so if they are present in the sample, they will be missed in the analysis [53]. The analysis in [64] still allows for a comparison between the liquid crystal enriched sample and the interfacial material. Both the interfacial material and the liquid crystal enriched material show an increase in oxygen and sulfur heteroatom contents when compared with asphaltenes [32]. It is possible that the materials are related. If so, then a portion of the liquid crystal forming material may play a role in water-oil emulsion stabilization. Figures 5-8 through 5-10 show DBE vs carbon number plots for some heteroatom classes of bitumen-water interfacial material [64]. On each figure the area for the liquid crystal enriched sample is circled. There is significant overlap between these two samples, especially in the O_1 and SO_2 heteroatom classes. It may be that some portion of the two samples are the same and further study into this area is warranted.

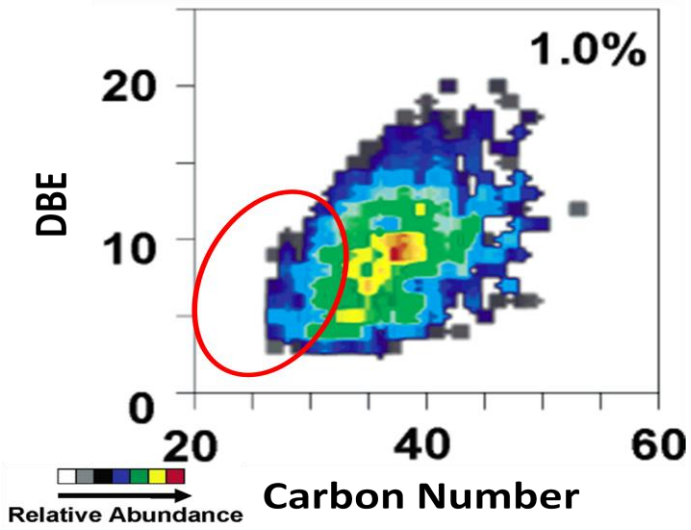

Figure 5-8. DBE vs Carbon number for O_1 class of bitumen-water interfacial material. Circled area shows approximately where the O_1 class is for the liquid crystal enriched sample. Adapted with permission from [64]. Copyright 2007 American Chemical Society.

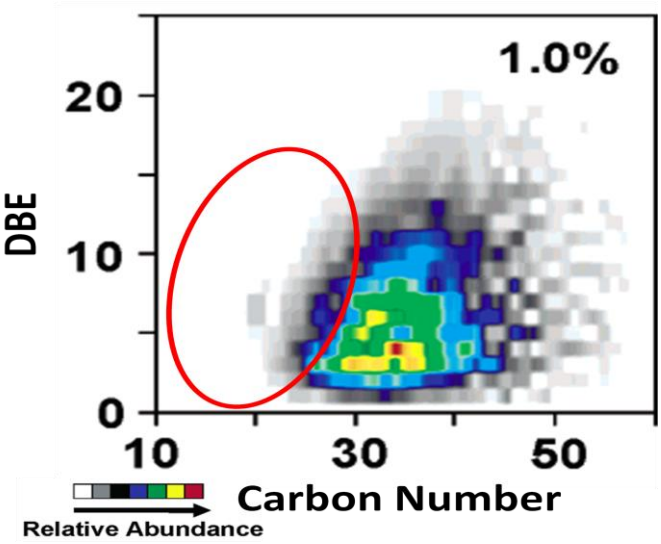

Figure 5-9. DBE vs Carbon number for O_2 class of bitumen-water interfacial material. Circled area shows approximately where the O_2 class is for the liquid crystal enriched sample. Adapted with permission from [64]. Copyright 2007 American Chemical Society.

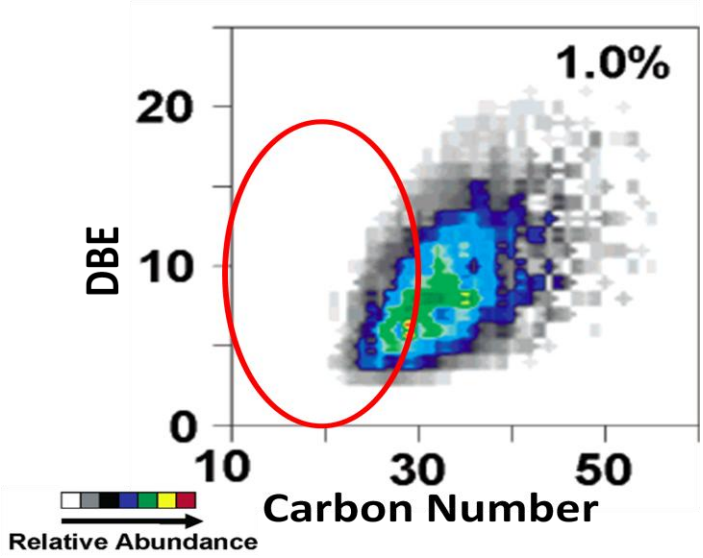

Figure 5-10. DBE vs Carbon number for SO_2 class of bitumen-water interfacial material. Circled area shows approximately where the SO_2 class is for the liquid crystal enriched sample. Adapted with permission from [64]. Copyright 2007 American Chemical Society.

From the FT-ICR MS analysis it is evident that the liquid crystal enriched sample remains complex with tens of thousands of compounds present. No single compound is responsible for the liquid crystalline behaviour exhibited by the sample. Further, combinations of molecules that do not form liquid crystals on their own can form liquid crystals in a mixture [65]. While specific compounds were not isolated from the liquid crystal enriched materials, known liquid crystal forming compounds listed in Table 2-1 fit the nominal molar mass range and belong to the major heteroatom classes found in the liquid crystal enriched sample. Examples are listed in Table 5-1 and are overlaid on DBE and H:C ratio vs carbon number plots by heteroatom class in Figures 5-11 to 5-17. All of these compounds are either plausible constituents of the liquid crystal enriched sample or become so with minor modification to end chain length or aromatic/naphthenic structure with the possible exception of the N_1 class liquid crystal compound, $C_{24}H_{33}N$ – Figure 5-13.

Table 5-1. Liquid crystal compounds from Table 2-1 divided into heteroatom classes.

Compound	DBE	H:C
HC Class		
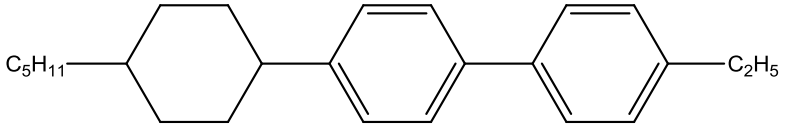 $C_{25}H_{34}$	9	1.36
S_1 Class		

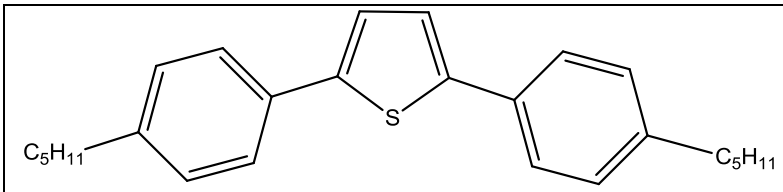 $C_{26}H_{32}S$	11	1.23
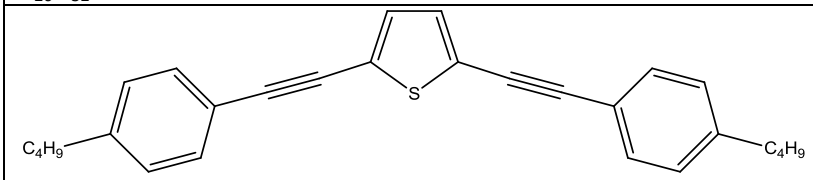 $C_{28}H_{28}S$	15	1
N_1 Class		
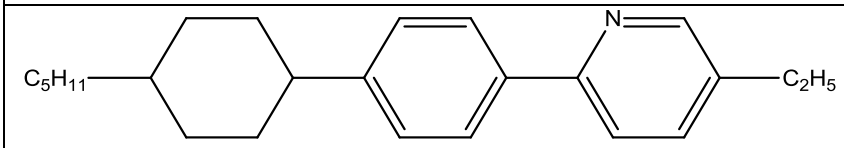 $C_{24}H_{33}N$	9	1.38
O_1 Class		
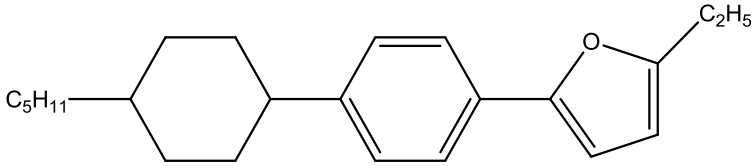 $C_{23}H_{32}O$	8	1.39
O_2 Class		
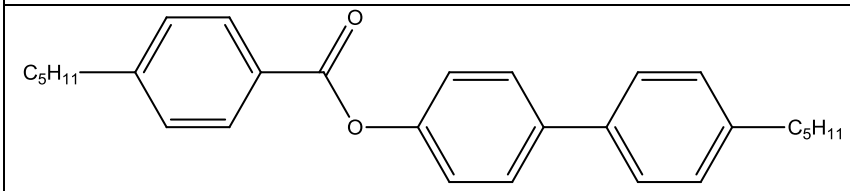 $C_{29}H_{34}O_2$	13	1.17
SO Class		
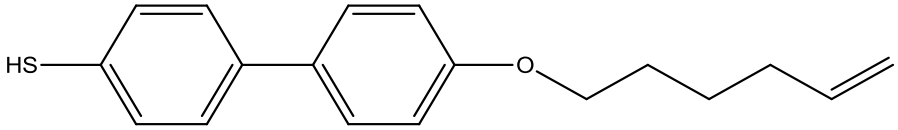 $C_{18}H_{20}OS$	9	1.11
SO_2 Class		
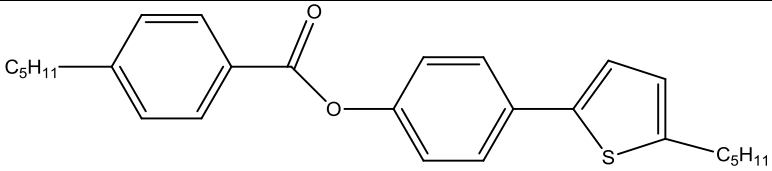 $C_{27}H_{32}O_2S$	12	1.19

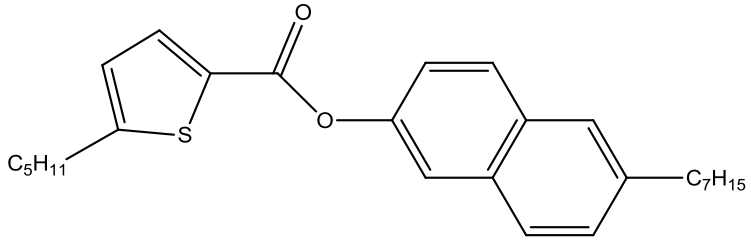 $C_{27}H_{34}O_2S$	11	1.26

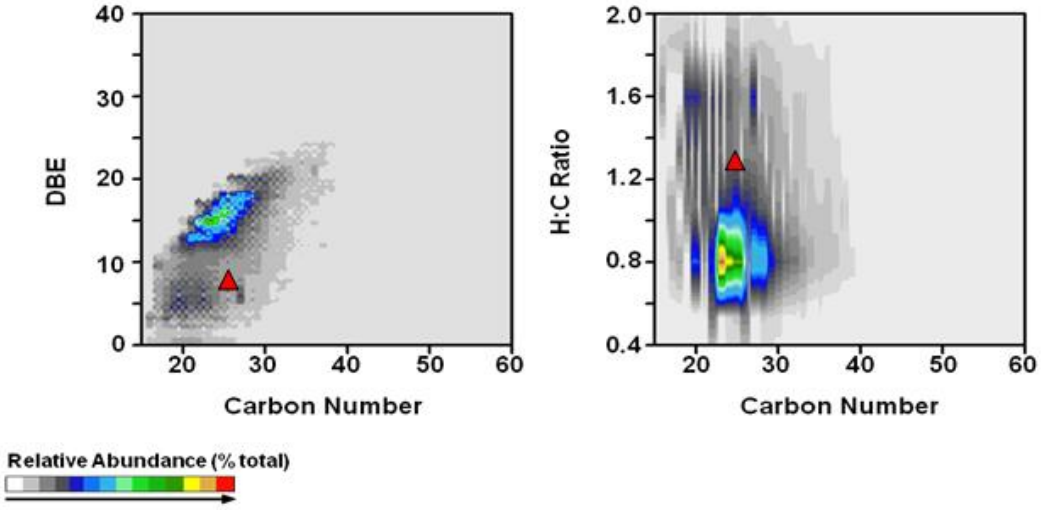

Figure 5-11. DBE and H:C plots for HC class for the liquid crystal enriched sample. The HC class liquid crystal, $C_{25}H_{34}$, is shown by the red triangle.

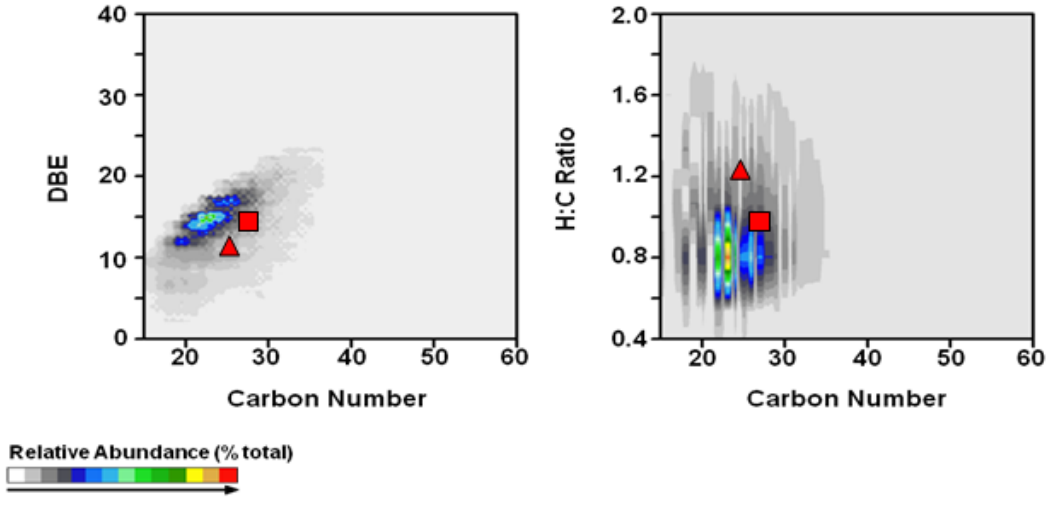

Figure 5-12. DBE and H:C plots for S_1 class for the enriched sample with S_1 liquid crystals included. Triangle: $C_{26}H_{32}S$. Square: $C_{28}H_{28}S$.

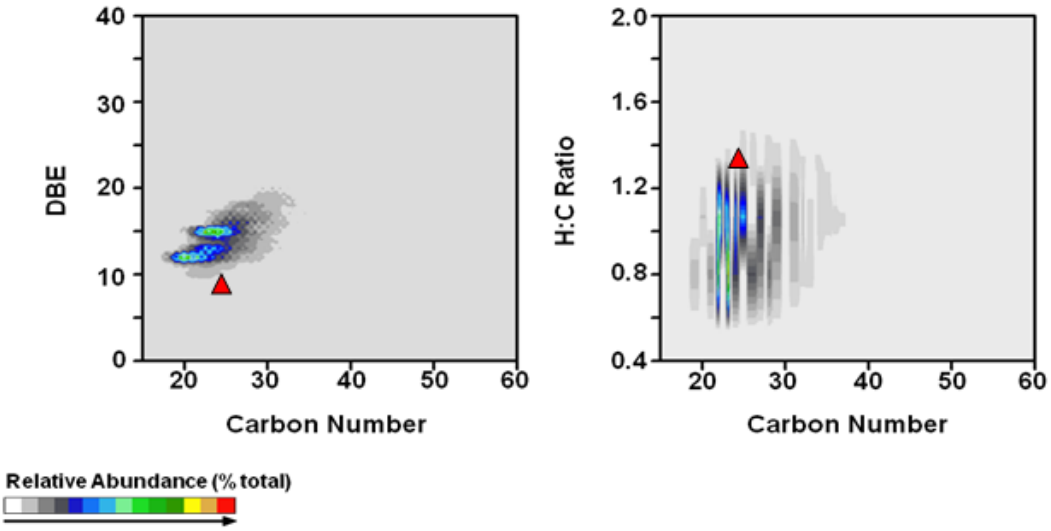

Figure 5-13. DBE and H:C plots for N_1 class for the enriched sample. Triangle shows the N_1 liquid crystal compound, $C_{24}H_{33}N$.

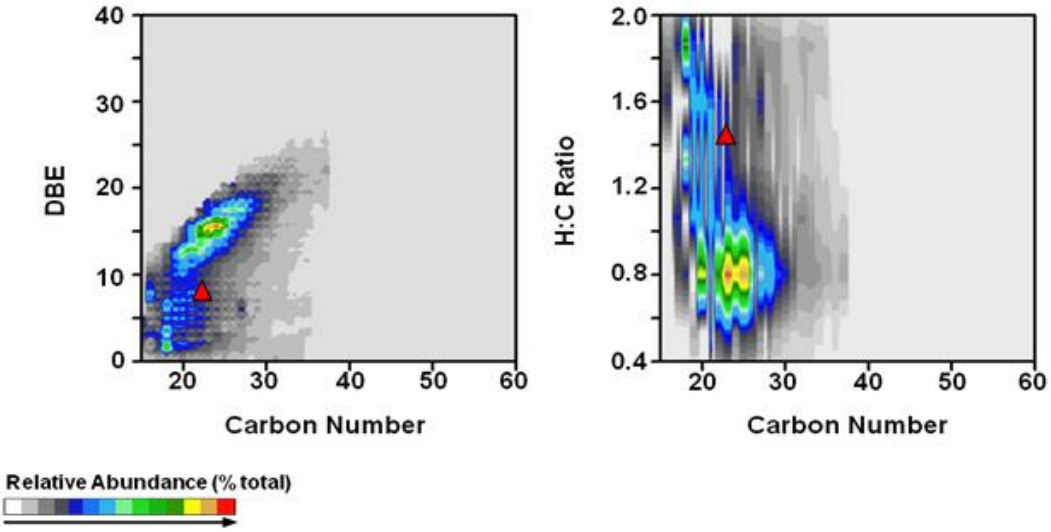

Figure 5-14. DBE and H:C plots for O_1 class for the enriched sample with O_1 liquid crystals included. Triangle: $C_{23}H_{32}O$.

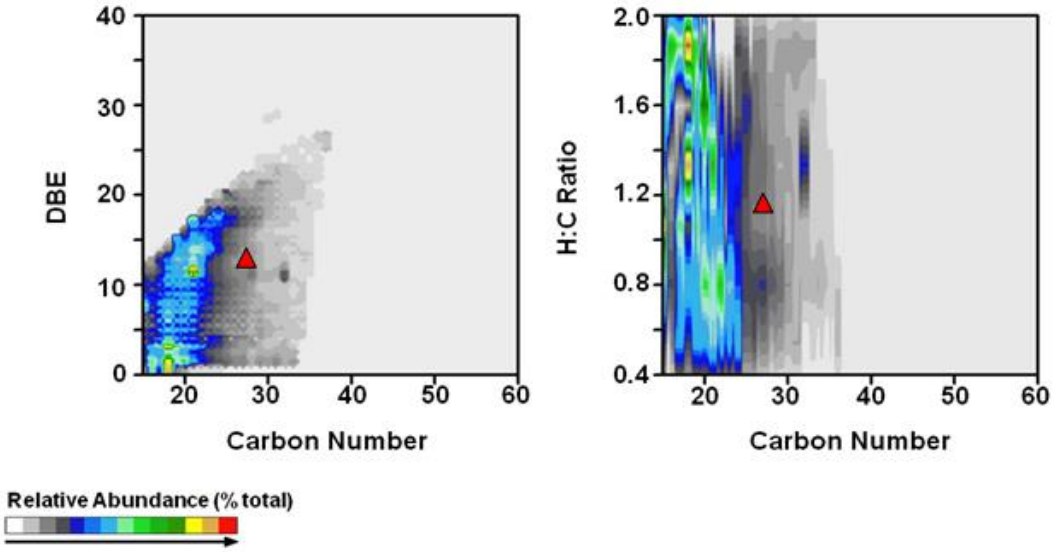

Figure 5-15. DBE and H:C plots for O_2 class for the enriched sample with O_2 class liquid crystal compound, $C_{29}H_{34}O_2$, shown by triangle.

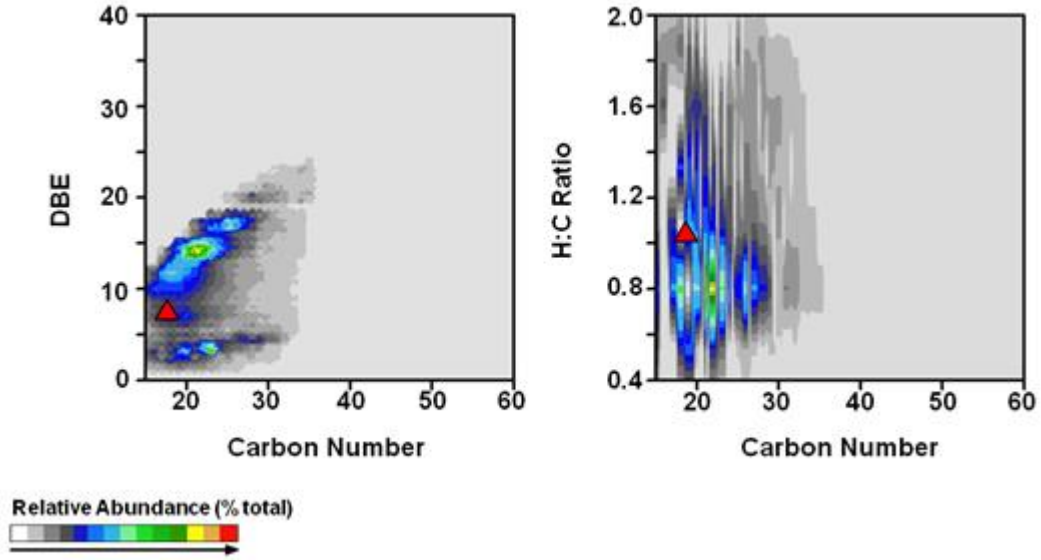

Figure 5-16. DBE and H:C plots for SO class for the enriched sample with SO class liquid crystal included. $C_{18}H_{20}OS$ shown by triangle.

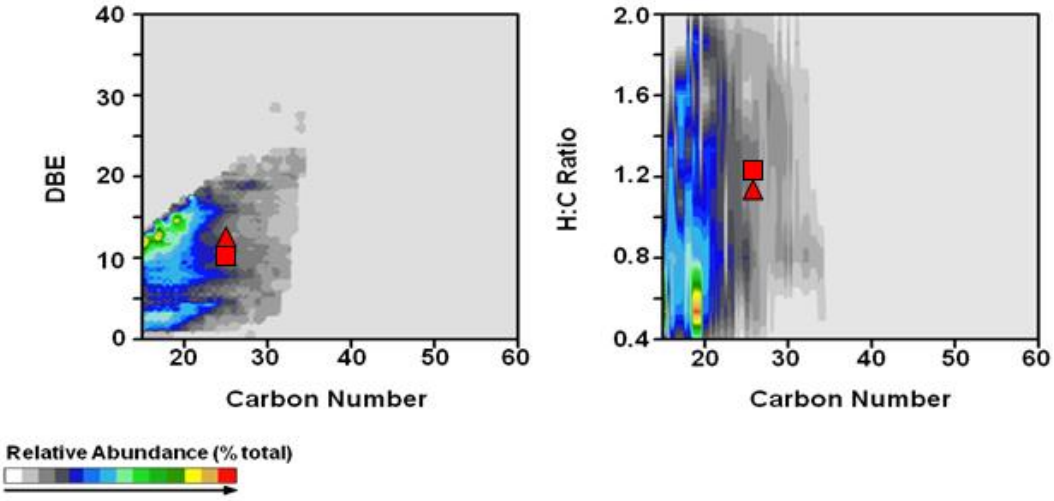

Figure 5-17. DBE and H:C plots for SO_2 class for the enriched sample with SO_2 class liquid crystals included. Triangle: $C_{27}H_{32}O_2S$. Square: $C_{27}H_{34}O_2S$.

6. Conclusions and Future Work

Conclusions

Liquid crystals, tentatively identified as smectic liquid crystals, were found to be present in all heavy petroleum fractions examined. The relative amounts present varied, with the enriched sample extracted from Athabasca bitumen C5 asphaltenes > SFE6 > C5 asphaltenes. The relative mass fraction in the Athabasca bitumen pentane maltenes was not determined. The appearance and disappearance temperatures also varied from sample type to sample type.

Quantification of the mass fraction of liquid crystal present using DSC measurements was inhibited by the coincidence of energetically large glass or other bulk transitions in samples at temperatures where the liquid crystals form. Parsing the two signals presents experimental challenges beyond the scope of this work but the subject will be pursued as a topic for future investigation. At higher temperatures, where the liquid crystals dissolve into or form an isotropic phase, the DSC signal is significantly weaker and can be either positive or negative depending mass fraction of liquid crystals present. This latter signal provides only a qualitative indicator of composition, at best.

Liquid crystals form irreversibly and preferentially on the exterior surfaces of asphaltene or maltene particles as they soften or melt creating biplex objects comprising an isotropic core surrounded by a liquid crystal layer. The nominal diameter of these objects is linked to the original size of the particles comprising the samples - less than ~ 150 um for the cases evaluated. From the PA-IR (standard and depth profiling) measurements, the liquid crystal forming materials migrate to the exterior surface (in most cases). The particles are not macroscopically heterogeneous initially. It is not clear at this time if the liquid crystal forming materials are part of the bulk or are nanodispersed initially. If the liquid crystals are heated to the point where they become isotropic (by dissolution or melting), they do not reappear on cooling, and only reappear on subsequent heating if the sample is crushed. DSC and PA-IR measurements, and polarized light microscopy observations all show that crushing a sample resets the liquid crystal formation behaviour.

The presence of liquid crystals on the exterior surface of particles facilitated the extraction of a liquid crystal enriched sample from a heat treated C5 asphaltene sample using a mixture of heptane + 10 vol % toluene. Liquid crystals were selectively removed from asphaltene particle surfaces.

Analysis of the liquid crystal enriched sample, produced from C5 asphaltenes, using FT-ICR MS showed increased abundances of sulfur, oxygen and nitrogen heteroatoms relative to asphaltenes and a significantly lower molar mass range than found for

asphaltenes. For the molar mass and DBE/H:C ratio ranges and heteroatom classes present, examples of liquid crystal forming compounds were identified. Molecules of these types and/or combinations of molecules that do not in themselves form liquid crystals are clearly present in the liquid crystal rich material.

Future Work

- Develop and scale-up liquid crystal extraction techniques based on solvent washing of particles (asphaltenes, maltenes, or other fractions). This would permit elemental analysis to confirm and quantify the extent of SNO enrichment in the liquid crystals, permit evaluation of the impact of their removal on bitumen processing, permit evaluation of possible recovery of additional or new materials bitumen/heavy oil.
- Investigate the link between the water-oil interfacial material and the liquid crystal forming materials.
- Quantify the mass fraction of liquid crystals in petroleum fractions

1. Andrews, A.B., R.E. Guerra, O.C. Mullins, and P.N. Sen, *Diffusivity of Asphaltene Molecules by Fluorescence Correlation Spectroscopy.* The Journal of Physical Chemistry A, 2006. **110**(26): p. 8093-8097.
2. Groenzin, H. and O.C. Mullins, *Asphaltene Molecular Size and Structure.* The Journal of Physical Chemistry A, 1999. **103**(50): p. 11237-11245.
3. Groenzin, H. and O.C. Mullins, *Molecular Size and Structure of Asphaltenes from Various Sources.* Energy & Fuels, 2000. **14**(3): p. 677-684.
4. Herod, A.A., K.D. Bartle, and R. Kandiyoti, *Characterization of heavy hydrocarbons by chromatographic and mass spectrometric methods: An overview.* Energy & Fuels, 2007. **21**(4): p. 2176-2203.
5. Herod, A.A., K.D. Bartle, and R. Kandiyoti, *Comment on a Paper by Mullins, Martinez-Haya, and Marshall "Contrasting Perspective on Asphaltene Molecular Weight. This Comment vs the Overview of A. A. Herod, K. D. Bartle, and R. Kandiyoti".* Energy & Fuels, 2008. **22**(6): p. 4312-4317.
6. Martínez-Haya, B., A.R. Hortal, P. Hurtado, M.D. Lobato, and J.M. Pedrosa, *Laser desorption/ionization determination of molecular weight distributions of polyaromatic carbonaceous compounds and their aggregates.* Journal of Mass Spectrometry, 2007. **42**(6): p. 701-713.
7. Mullins, O.C., B. Martinez-Haya, and A.G. Marshall, *Contrasting perspective on asphaltene molecular weight. This comment vs the overview of A. A. Herod, K. D. Bartle, and R. Kandiyoti.* Energy & Fuels, 2008. **22**(3): p. 1765-1773.
8. Qian, K., K.E. Edwards, M. Siskin, W.N. Olmstead, A.S. Mennito, G.J. Dechert, and N.E. Hoosain, *Desorption and Ionization of Heavy Petroleum Molecules and Measurement of Molecular Weight Distributions.* Energy & Fuels, 2007. **21**(2): p. 1042-1047.
9. Wargadalam, V.J., K. Norinaga, and M. Iino, *Size and shape of a coal asphaltene studied by viscosity and diffusion coefficient measurements.* Fuel, 2002. **81**(11-12): p. 1403-1407.
10. Akbarzadeh, K., A. Hammami, A. Kharrat, D. Zhang, S. Allenson, J. Creek, S. Kabir, A. Jamaluddin, A.G. Marshall, R.P. Rodgers, O.C. Mullins, and T. Solbakken, *Asphaltenes - Problematic but rich in potential.* Oilfield Review, 2007. **19**(2): p. 22-43.
11. Gawel, I., D. Bociarska, and P. Biskupski, *Effect of asphaltenes on hydroprocessing of heavy oils and residua.* Applied Catalysis A: General, 2005. **295**(1): p. 89-94.
12. Bagheri, S.R., A. Bazyleva, M.R. Gray, W.C. McCaffrey, and J.M. Shaw, *Observation of Liquid Crystals in Heavy Petroleum Fractions.* Energy & Fuels, 2010. **24**: p. 4327-4332.
13. de Gennes, P.G. and J. Prost, *The physics of liquid crystals*. 2nd ed. The International Series of Monographs on Physics, ed. J. Birman, et al. 1993, New York: Oxford University Press. 597.
14. Simon, J., P. Bassoul, and S. Norvez, *Molecular materials. III. Towards opto-electronics finalities.* New J. Chem., 1989. **13**(1): p. 13-31.
15. *Introduction to liquid crystals*. [cited 2011 July 7]; Available from: http://barrett-group.mcgill.ca/teaching/liquid_crystal/LC04.htm

http://barrett-group.mcgill.ca/teaching/liquid_crystal/LC02.htm.

16. Campbell, N.L., W.L. Duffy, G.I. Thomas, J.H. Wild, S.M. Kelly, K. Bartle, M. O'Neill, V. Minter, and R.P. Tuffin, *Nematic 2,5-disubstituted thiophenes.* Journal of Materials Chemistry, 2002. **12**(9): p. 2706-2721.
17. Petrov, V.F. and A.I. Pavluchenko, *Furan as a structural fragment in liquid crystals.* Molecular Crystals and Liquid Crystals, 2003. **393**: p. 1-13.
18. Wilderbeek, H.T.A., M.G.M. van der Meer, M.A.G. Jansen, L. Nelissen, H.R. Fischer, J.J.G.S. Van Es, C.W.M. Bastiaansen, J. Lub, and D.J. Broer, *Synthesis and properties of phenyl benzoate-based and biphenyl-based liquid crystalline thiol-ene monomers.* Liquid Crystals, 2003. **30**(1): p. 93.
19. Armarego, W.L.F. and C.L.L. Chai, *Purification of Laboratory Chemicals (6th Edition)*. 2009, Elsevier. p. 14-16.
20. Liberko, C.A. and J. Shearer, *Preparation of a surface-oriented liquid crystal - An experiment for the undergraduate organic chemistry laboratory.* Journal of Chemical Education, 2000. **77**(9): p. 1204-1205.
21. Verbit, L., *LIQUID-CRYSTALS - SYNTHESIS AND PROPERTIES - EXPERIMENT FOR INTEGRATED ORGANIC AND PHYSICAL LABORATORY.* Journal of Chemical Education, 1972. **49**(1): p. 36-&.
22. Haberfel.Jl, E.C. Hsu, and J.F. Johnson, *LIQUID-CRYSTAL PURIFICATION BY ZONE-REFINING.* Molecular Crystals and Liquid Crystals, 1973. **24**(1-2): p. 1-5.
23. Didchenko, R., *LIQUID CRYSTALS IN CARBONACEOUS MATERIALS.* American Chemical Society, Polymer Preprints, Division of Polymer Chemistry, 1977. **18**(Compendex): p. 81-83.
24. Gasparoux, H., C. Destrade, and G. Fug, *CARBONACEOUS MESOPHASE AND DISC-LIKE LIQUID CRYSTALS.* Molecular Crystals and Liquid Crystals, 1980. **59**(Compendex): p. 109-116.
25. Hurt, R.H. and Y. Hu, *Thermodynamics of carbonaceous mesophase.* Carbon, 1999. **37**(2): p. 281-292.
26. Marsh, H. and C.S. Latham. *CHEMISTRY OF MESOPHASE FORMATION*. in *Petroleum-Derived Carbons. Papers based on presentations at the 187th National ACS Meeting.* 1986. Washington, DC, USA: ACS.
27. Sanada, Y., T. Furuta, H. Kimura, and H. Honda, *Formation of anisotropic mesophase from various carbonaceous materials in early stages of carbonization.* Fuel, 1973. **52**(2): p. 143-148.
28. Singer, L.S. *MESOPHASE IN CARBONACEOUS PITCHES*. in *Polymer Liquid Crystals.* 1985. Cambridge, Engl: Royal Soc of Chemistry.
29. Horvath-Svabo, G., J.H. Masliyah, and J. Czarnecki, *Friberg correlations in oil recovery.* Journal of Dispersion Science and Technology, 2006. **27**(5): p. 625-633.
30. Dauche, F.M., G. Bolanos, A. Blasig, and M.C. Thies, *Control of mesophase pitch properties by supercritical fluid extraction.* Carbon, 1998. **36**(7-8): p. 953-961.
31. Chung, K.H., C. Xu, M. Gray, Y. Zhao, L. Kotlyar, and B.D. Sparks, *The chemistry, reactivity, and processability of Athabasca bitumen pitch.* Reviews in Process Chemistry and Engineering, 1998. **1**: p. 41-79.
32. Czarnecki, J., *Stabilization of Water in Crude Oil Emulsions. Part 2.* Energy & Fuels, 2009. **23**: p. 1253-1257.
33. Rahmani, S., W. McCaffrey, and M.R. Gray, *Kinetics of Solvent Interactions with Asphaltenes during Coke Formation.* Energy & Fuels, 2001. **16**(1): p. 148-154.
34. Borton, D., D.S. Pinkston, M.R. Hurt, X.L. Tan, K. Azyat, A. Scherer, R. Tykwinski, M. Gray, K.N. Qian, and H.I. Kenttamaa, *Molecular Structures of Asphaltenes*

Based on the Dissociation Reactions of Their Ions in Mass Spectrometry. Energy & Fuels, 2010. **24**: p. 5548-5559.

35. Groenzin, H. and O. Mullins, *MOLECULAR SIZE AND STRUCTURE OF ASPHALTENES.* Petroleum Science & Technology, 2001. **19**(1/2): p. 219.
36. Mullins, O.C., *Petroleomics and Structure–Function Relations of Crude Oils and Asphaltenes*

Asphaltenes, Heavy Oils, and Petroleomics, O.C. Mullins, et al., Editors. 2007, Springer New York. p. 1-16.

37. Mullins, O.C., *The Modified Yen Model†.* Energy & Fuels, 2010. **24**(4): p. 2179-2207.
38. Rodgers, R.P., A.C. Lazar, P.T.A. Reilly, W.B. Whitten, and J.M. Ramsey, *Direct Determination of Soil Surface-Bound Polycyclic Aromatic Hydrocarbons in Petroleum-Contaminated Soils by Real-Time Aerosol Mass Spectrometry.* Analytical Chemistry, 2000. **72**(20): p. 5040-5046.
39. Ruiz-Morales, Y. and O.C. Mullins, *Polycyclic Aromatic Hydrocarbons of Asphaltenes Analyzed by Molecular Orbital Calculations with Optical Spectroscopy.* Energy & Fuels, 2006. **21**(1): p. 256-265.
40. McKenna, A.M., J.M. Purcell, R.P. Rodgers, and A.G. Marshall, *Identification of Vanadyl Porphyrins in a Heavy Crude Oil and Raw Asphaltene by Atmospheric Pressure Photoionization Fourier Transform Ion Cyclotron Resonance (FT-ICR) Mass Spectrometry.* Energy & Fuels, 2009. **23**(4): p. 2122-2128.
41. Trejo, F., G. Centeno, and J. Ancheyta, *Precipitation, fractionation and characterization of asphaltenes from heavy and light crude oils.* Fuel, 2004. **83**(16): p. 2169-2175.
42. Yang, M.G. and S. Eser, *Fractionation and molecular analysis of vacuum-residue asphaltenes.* Abstracts of Papers of the American Chemical Society, 1999. **218**: p. U625-U625.
43. Kaminski, T.J., H.S. Fogler, N. Wolf, P. Wattana, and A. Mairal, *Classification of asphaltenes via fractionation and the effect of heteroatom content on dissolution kinetics.* Energy & Fuels, 2000. **14**(1): p. 25-30.
44. Sigma-Aldrich. *4-Isothiocyanatophenyl 4-pentylbicyclo[2.2.2]octane-1-carboxylate* 2011 [cited 2011 August 22, 2011]; Manufacturer's page for chemical]. Available from: http://www.sigmaaldrich.com/catalog/ProductDetail.do?lang=en&N4=370053|ALDRICH&N5=SEARCH_CONCAT_PNO|BRAND_KEY&F=SPEC.
45. McKenna, A.M., *Telephone conversation with author*. 2011.
46. Crabtree, R.H. and D.M.P. Mingos, *Comprehensive Organometallic Chemistry III, Volumes 1 - 13*. 2007, Elsevier. p. 208-209.
47. *Smectic A - Nematic phase transition*. 2004 [cited 2011 July 8]; Available from: http://commons.wikimedia.org/wiki/File:Smectic_nematic.jpg.
48. Patnaik, P., *Dean's Analytical Chemistry Handbook (2nd Edition)*. 2004, McGraw-Hill.
49. Michaelian, K.H., *Photoacoustic Infrared Spectroscopy*. 1 ed. Chemical Analysis, ed. J.D. Winefordner. 2003, Hoboken, New Jersey: John Wiley & Sons. 335.
50. Michaelian, K.H., R.H. Hall, and K.I. Kenny, *Photoacoustic infrared spectroscopy of Syncrude post-extraction oil sand.* Spectrochimica Acta Part A: Molecular and Biomolecular Spectroscopy, 2006. **64**(3): p. 703-710.

51. Wen, Q. and K.H. Michaelian, *Photoacoustic infrared spectroscopy of polymer beads.* Spectrochimica Acta Part a-Molecular and Biomolecular Spectroscopy, 2009. **73**(5): p. 823-827.
52. Marshall, A.G. and C.L. Hendrickson, *Fourier transform ion cyclotron resonance detection: principles and experimental configurations.* International Journal of Mass Spectrometry, 2002. **215**(1-3): p. 59-75.
53. Purcell, J.M., C.L. Hendrickson, R.P. Rodgers, and A.G. Marshall, *Atmospheric Pressure Photoionization Fourier Transform Ion Cyclotron Resonance Mass Spectrometry for Complex Mixture Analysis.* Analytical Chemistry, 2006. **78**(16): p. 5906-5912.
54. Hsu, C.S., C.L. Hendrickson, R.P. Rodgers, A.M. McKenna, and A.G. Marshall, *Petroleomics: advanced molecular probe for petroleum heavy ends.* Journal of Mass Spectrometry, 2011. **46**(4): p. 337-343.
55. Marshall, A.G., C.L. Hendrickson, and G.S. Jackson, *Fourier transform ion cyclotron resonance mass spectrometry: A primer.* Mass Spectrometry Reviews, 1998. **17**(1): p. 1-35.
56. McKenna, A.M., J.M. Purcell, R.P. Rodgers, and A.G. Marshall, *Heavy Petroleum Composition. 1. Exhaustive Compositional Analysis of Athabasca Bitumen HVGO Distillates by Fourier Transform Ion Cyclotron Resonance Mass Spectrometry: A Definitive Test of the Boduszynski Model.* Energy & Fuels, 2010. **24**(5): p. 2929-2938.
57. Marshall, A.G. and R.P. Rodgers, *Petroleomics: Chemistry of the underworld.* Proceedings of the National Academy of Sciences, 2008.
58. McKenna, A.M., G.T. Blakney, F. Xian, P.B. Glaser, R.P. Rodgers, and A.G. Marshall, *Heavy Petroleum Composition. 2. Progression of the Boduszynski Model to the Limit of Distillation by Ultrahigh-Resolution FT-ICR Mass Spectrometry.* Energy & Fuels, 2010. **24**(5): p. 2939-2946.
59. Dãbrowski, R., J. Dziaduszek, W. Drzewiński, K. Czupryński, and Z. Stolarz, *Synthesis and Mesomorphic Characteristic of Bicyclo-(2,2,2)Octane Derivatives with the -NCS Terminal Group.* Molecular Crystals and Liquid Crystals Incorporating Nonlinear Optics, 1990. **191**(1): p. 171-176.
60. Acree, W.E. and J.S. Chickos, *Phase change enthalpies and entropies of liquid crystals.* Journal of Physical and Chemical Reference Data, 2006. **35**(3): p. 1051-1330.
61. Bazyleva, A., M. Fulem, M. Becerra, B. Zhao, and J.M. Shaw, *Phase Behavior of Athabasca Bitumen.* Journal of Chemical & Engineering Data, 2011. **56**(7): p. 3242-3253.
62. Nikooyeh, K. and J.M. Shaw. *Phase Behavior of Asphaltenes + Organic Diluents*. in *22nd Thermodynamics Conference*. 2011. Athens, Greece.
63. Zhang, Y., T. Takanohashi, S. Sato, T. Kondo, I. Saito, and R. Tanaka, *Dissolution and dilution of asphaltenes in organic solvents.* Energy & Fuels, 2003. **17**(1): p. 101-106.
64. Stanford, L.A., R.P. Rodgers, A.G. Marshall, J. Czarnecki, and X.A. Wu, *Compositional characterization of bitumen/water emulsion films by negative- and positive-ion electrospray ionization and field desorption/ionization Fourier transform ion cyclotron resonance mass spectrometry.* Energy & Fuels, 2007. **21**(2): p. 963-972.

65. Brown, G.H. and W.G. Shaw, *THE MESOMORPHIC STATE - LIQUID CRYSTALS.* Chemical Reviews, 1957. **57**(6): p. 1049-1157.